ORIGINAL ARTICLE

Inconsistent Atlantic Links to Precipitation Extremes over the Humid Tropics

Hyacinth C. Nnamchi[1] · Ismaila Diallo[2]

Abstract

This study investigates extreme wet and dry conditions over the humid tropics and their connections to the variability of the tropical ocean basins using observations and a multi-model ensemble of 24 state-of-the-art coupled climate models, for the 1930–2014 period. The extreme wet (dry) conditions are consistently linked to Central Pacific La Niña (Eastern Pacific El Niño), the weakest being the Congo basin, and homogeneous patterns of sea surface temperature (SST) variability in the tropical Indian Ocean. The Atlantic exhibits markedly varying configurations of SST anomalies, including the Atlantic Niño and pan-Atlantic decadal oscillation, with non-symmetrical patterns between the wet and dry conditions. The oceanic influences are associated with anomalous convection and diabatic heating partly related to variations in the strength of the Walker Circulation. The observed connection between the Amazon basin, as well as the Maritime continent, and the Indo-Pacific variability are better simulated than that of the Congo basin. The observed signs of the Pacific and Indian SST anomalies are reversed for the modelled Congo basin extreme conditions which are, instead, tied to the Atlantic Niño/Niña variability. This Atlantic–Congo basin connection is related to a too southerly location of the simulated inter-tropical convergence zone that is associated with warm SST biases over the Atlantic cold tongue. This study highlights important teleconnections and model improvements necessary for the skillful prediction of extreme precipitation over the humid tropics.

Keywords ENSO · Atlantic variability · Basins interaction · Extreme conditions · Humid tropics · CMIP6

1 Introduction

The humid tropics represent the tropical rainforest climate of the Köppen–Geiger classification. It is found in South America, Africa, and Asia, corresponding to the Amazon Basin, Congo Basin, and Maritime Continent, respectively (Beck et al. 2018; marked by boxes in Fig. 1a). Precipitation and temperatures are high throughout the year, with small annual temperature ranges (Fig. 1b–d). Deep convection and diabatic heating, representing the upward branches of the Walker Circulation, over the humid tropics drive the global-scale tropical atmospheric circulation (Webster 1983; Washington et al. 2013; Hart et al. 2019). Specifically, the

highest annual precipitation over the humid tropics are associated with the rising cells of the Walker Circulation over the Amazon Basin, Congo Basin, and Maritime Continent, respectively (Fig. 1a). These regions are linked by the inter-tropical convergence zone (ITCZ) as shown by the band of the maximum precipitation rates over the tropics (contours in Fig. 1a). As such, variations in tropical circulations can induce precipitation anomalies, leading to extreme hydro-climatic events such as droughts and floods. These extreme events profoundly affect the local hydrology, ecosystem services, and livelihoods of the people (Dikshit et al. 2020; Shi et al. 2020; Kirono et al. 2020).

The frequency, duration, and intensity of extreme hydro-climate events have generally been increasing in recent years over the tropics (Marengo et al. 2011; Kim et al. 2019; Ajayi and Ilori 2020; Cook et al. 2020; Almazroui et al. 2021a; Klutse et al. 2021; Robinson et al. 2021; Nicholson et al. 2022; Lau et al. 2023), and are associated with long-lived organised mesoscale convective systems (Roca and Fiolleau 2020). These are often accompanied by disasters associated

✉ Hyacinth C. Nnamchi
hnnamchi@geomar.de

[1] GEOMAR Helmholtz Centre for Ocean Research Kiel, Wischhofstraße 1-3, 24148 Kiel, Germany

[2] Department of Meteorology and Atmospheric Science, The Pennsylvania State University, University Park, PA 16802, USA
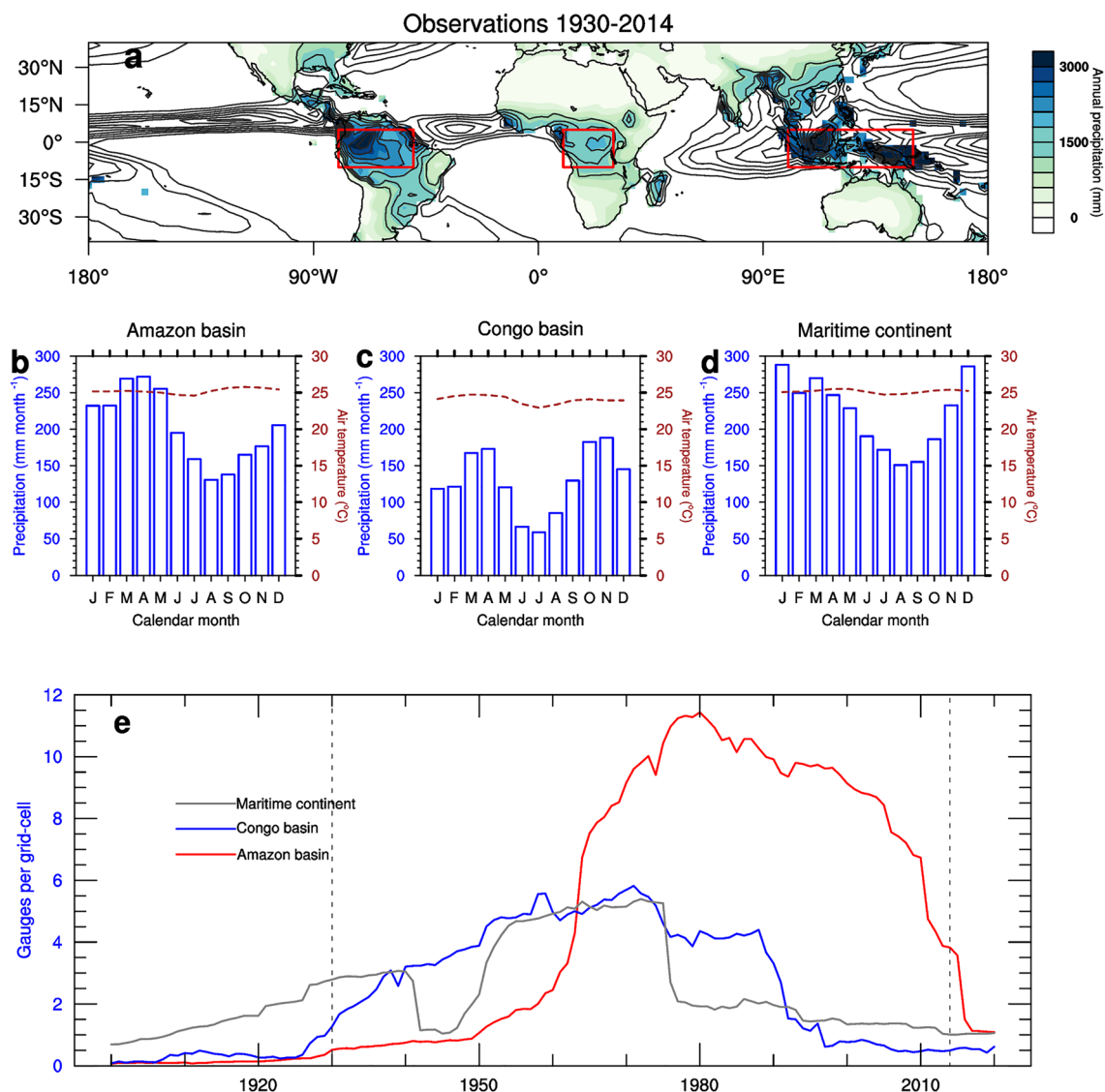
Fig. 1 a Mean annual precipitation from GPCC 1930–2014, whereas the contours show the monthly-mean precipitation rates in mm day^{-1} from the GPCP satellite-derived dataset 1979–2014 (only values of 3 mm day^{-1} are contoured at the interval of 1 mm day^{-1}). **b–d** (left axis) annual cycle of land precipitation (bar plots) averaged over the Amazon basin (5° N–10° S, 50–80° W), Congo basin (5° N–10° S, 10–30° E), and Maritime continent (5° N–10° S, 100–150° E) shown by the red boxes in **a**. The right axis in **b–d** shows the annual cycle of 2-m air temperature represented by the dashed line. **e** Number of rain gauges within a grid-cell averaged over the Amazon basin (red), Congo basin (blue), and Maritime continent (grey). Dashed vertical lines in **e** delineate the study period 1930–2014. Note that for the area-average over the humid tropic regions, only land grid points included to the boxes are considered

with severe droughts and floods (Kooperman et al. 2018; Rowland et al. 2015).

Several recent studies have investigated the occurrences of hydroclimate extremes over the Congo basin (Hua et al. 2016; Cook et al. 2020; Dyer et al. 2017; Nicholson et al. 2022), the Amazon basin (Marengo and Espinoza 2016; Kooperman et al. 2018), and the Maritime continent (Kim et al. 2019; Da Silva and Matthews 2021; Strnad et al. 2023). Focusing over the 1979–2014 periods, Hua et al. (2016) have shown that the observed drying trend was strongest and statistically significant during the boreal

spring (April–May–June) in the eastern part of the Congo basin. Nicholson et al. (2022) reported wetter conditions spanning the years 2016–2020 in the Congo Basin. They concluded that the wetter conditions were associated with an increase in total column water vapor and in convective available potential energy. The important role of moisture flux convergence (divergence) in promoting wet (dry) conditions over the Congo basin have been investigated using climate models (Washington et al. 2013; Hua et al. 2018; Tamoffo et al. 2019).

The Amazon basin is particularly susceptible to droughts under a changing climate (Kooperman et al. 2018; Marengo and Espinoza 2016; Seneviratne et al. 2012; Cox et al. 2008), as well as drying trends (Almazroui et al. 2021b). For instance, since the end of the last century, the Amazon basin has experienced several extreme droughts (Marengo and Espinoza 2016; Erfanian et al. 2017). Modelling studies have reported systematic dry biases when simulating precipitation variability over the Amazon basin (Gulizia and Camilloni 2015), and these biases have been related to the tropical sea surface temperature (SST) in the CMIP5 models (Villamayor et al. 2018). Extreme precipitation is quite common in the Maritime continent, leading to devastating floods (Rodysill et al. 2019) which represents about 30% of the natural disasters in Indonesia (Dewata and Umar 2019), and causing profound societal impacts (Adhikari et al. 2010; Da Silva and Matthews 2021).

Understanding the drivers of the tropical circulation, leading to extreme precipitation is, therefore, key to advancing climate predictions over the humid tropics. The El Niño Southern Oscillation (ENSO), the most important mode of interannual climate variability, drives global-scale atmospheric circulation variability (Bjerknes 1969; Philander et al. 1984; Ropelewski and Halpert 1987; Wang 2002; McPhaden et al. 2006; Erfanian et al. 2017; Cai et al. 2019). As strengthening (weakening) of the Walker circulation implies stronger (weaker) of the mean ocean–atmosphere state, such that La Niña (El Niño) pattern in the tropical Pacific would lead to increases (decreases) in precipitation over the humid tropics. However, the atmospheric circulation and precipitation response to ENSO depend on the spatial configuration of the Pacific SST anomalies such as the Eastern Pacific versus Central Pacific events (Weng et al. 2009; Zheleznova and Gushchina 2017; Gushchina et al. 2020).

Furthermore, the tropical Indian and Atlantic Oceans have also been linked to precipitation variability over the humid tropical regions. Specifically, increased precipitation over the Amazon basin has been linked to the Atlantic meridional mode or the pan-Atlantic decadal oscillation (ADO), characterised by meridional gradients in SST and wind anomalies from the cold to the warm bands from the South Atlantic all the way to Greenland (Xie and Tanimoto 1998; Nnamchi et al. 2023). In the tropical Atlantic, the ADO pattern is defined by a cross-equatorial pattern of SST and wind anomalies in concert with the north–south movements of the inter-tropical convergence zone (ITCZ) referred to as the Atlantic meridional mode (AMM). Increases in precipitation over the Amazon basin are associated with cold SST anomalies over the tropical North Atlantic and warm SST anomalies over the tropical South Atlantic representing the negative phase of the AMM (Foltz et al. 2019; Servain et al. 1999; Yoon 2016;

Towner et al. 2020). This is associated with a southerly displacement of the ITCZ (Chang et al. 1997; Xie and Tanimoto 1998; Foltz et al. 2019; Nnamchi et al. 2023), and reduced (increased) moisture transport from tropical North Atlantic (tropical South Atlantic) to the Amazon (Marengo 1992; Drumond et al. 2014). In contrast, the positive phase of the AMM is characterized by the reversal of the SST and moisture transport anomalies leading to reduction in precipitation over the Amazon.

The Indian Ocean dipole (IOD), which is characterized by SST variability of opposite polarity between the western and eastern tropical Indian Ocean has been linked to precipitation anomalies over the Congo basin (Moihamette et al. 2022) and the Maritime continent (Xiao et al. 2022). The positive phase of the IOD is defined by warm (cold) SST anomalies in the western (eastern) tropical Indian Ocean and is associated with suppressed convection and reduced precipitation over the Maritime continent (Saji and Yamagata 2003; Xiao et al. 2022). On the other hand, positive IOD promotes wet conditions over the Congo basin region (Moihamette et al. 2022). The tropical Atlantic SST anomalies, through their impacts on the seasonal variability of the ITCZ, influence precipitation variability over the Congo basin (Nicholson 2009; Wang et al. 2021).

Here, we revisit the mechanism driving the occurrence of extreme precipitation conditions, i.e., dry and wet conditions, over the humid tropics. We focus on the respective humid tropical regions and investigate their connections to the tropical ocean basins generally, using monthly observational datasets and a multi-model 24-member ensemble of the Coupled Model Intercomparison Project phase 6 (CMIP6; Eyring et al. 2016) from 1930 to 2014. This approach allows us to directly link the extreme wet and dry conditions to the key oceanic variability globally. We also highlight the similarities and differences in the ocean–atmosphere variability associated with the different humid tropical regions. We find that the impacts of the Atlantic are inconsistent in observations, and the CMIP6 ensemble fails to capture this inconsistency, which potentially poses a problem for skillful seasonal climate prediction.

The rest of this paper is organized as follows. Section 2 describes the observational datasets, CMIP6 models, and analysis methods. Section 3 presents the results including the observations of the extreme wet and dry conditions as well as the underlying ocean–atmosphere variability. This section also contains an evaluation of the multi-model ensemble CMIP6 simulated extreme conditions, the related SST anomalies, and the ensemble-mean SST and precipitation biases. Discussion, limitations, and outlooks are presented in Sect. 4, the paper ends with Summary and concluding remarks in Sect. 5.

2 Data, Models, and Analysis Methods

2.1 Data

2.1.1 Precipitation Dataset

We analyze the gauge-derived Global Precipitation Climatology Centre (GPCC) Full Data Monthly Product Version 7.0 on $2.5° \times 2.5°$ longitude–latitude global grids (Schneider et al. 2014, 2017). The number of rain gauge stations per $2.5° \times 2.5°$ cell increased progressively from the early 1900s to reach a maximum around 1970 and around 1980 for the Congo basin and for the Amazon basin, respectively (Fig. 1e). Using a different data source, Washington et al. (2013) reported a decline in the number of gauges over the Congo basin between 1950 and 1980. The Amazon basin has the highest number of rain gauges per grid cell among the regions. The Maritime continent curve exhibits the most fluctuations, with a decline in the 1940s and then increases up to the mid-1970s. The number of gauges per grid cell displays a systematic decline since the 1970s/1980s for all three regions, which may be partly explained by time-lapse before historical data are included in the archives (Becker et al. 2013).

The past four decades denote the satellite era in global observations, with some products based on a combination of rain gauge measurements and satellite estimates of precipitation. The low density also limits opportunities to evaluate and calibrate satellite-based observations (Washington et al. 2013; Hewitson et al. 2014; Schneider et al. 2017). Here, we compare the GPCC with three other datasets that include satellite estimates, as well as the wholly rain gauge-derived Climatic Research Unit gridded Time Series (CRU hereafter) version 4.06 precipitation (Harris et al. 2020) on $0.5°$ latitude $\times 0.5°$ longitude grids, during the common period from 1981 to 2014. The satellite/gauge-based datasets are the Climate Hazards Group InfraRed Precipitation with Station data (CHIRPS) precipitation on $0.05°$ latitude $\times 0.05°$ longitude grids from $50°$ S to $50°$ N and all longitudes (Funk et al. 2015), the Climate Prediction Center (CPC) Merged Analysis of Precipitation on $2.5° \times 2.5°$ global grids (CMAP; Xie and Arkin 1997), and the version 3.1 of Global Precipitation Climatology Project (GPCP) analysis product on $2.5° \times 2.5°$ global grids (Adler et al. 2003). Overall, the GPCC precipitation averaged over the humid tropics exhibits both consistency and close correlations with the other products ($r \geq 0.90$; Fig. 2). The correlations appear insensitive to the horizontal resolution of the datasets, suggesting that using a different dataset may not change our conclusions.

2.1.2 Sea Surface Temperature Datasets

The variable quality of sea surface temperature (SST) measurement, limited areas of the oceans sampled, and the various statistical methods used to create globally complete grids constitute sources of uncertainty in SST datasets (Kennedy 2014). Here, we discuss the uncertainties in our results through the analysis of four different twentieth century gridded SST datasets. These are the Centennial In Situ Observation-Based Estimates of the Variability of SST and Marine Meteorological Variables (COBE) version 2 (Ishii et al. 2005), the Extended Reconstruction Sea Surface Temperature (ERSST) version 5 (Huang et al. 2017), United Kingdom Met Office Hadley Centre's sea ice and sea surface temperature dataset version 1.1 (HadISST; hereafter HadISST) (Rayner et al. 2003), and the Kaplan Extended SST (KAPLAN) version 2 (Kaplan et al. 1998).

The COBE data set is a spatially complete, interpolated monthly dataset on a $1° \times 1°$ horizontal latitude–longitude grids for 1850 to present. It combines SSTs from International Comprehensive Ocean–Atmosphere Data Set (ICOADS) release 2.5, the Japanese Kobe collection, and reports from ships and buoys, gridded using optimal interpolation (Kaplan et al. 1998). The ERSST is based on statistical interpolation of the ICOADS release 3.0 data, and argo float data in the recent years (since around 2000) and is available on a $2° \times 2°$ horizontal grids from 1854 to the present (Huang et al. 2017). The ERSST includes corrections to reconcile different measurement types (ship engine room intakes, ship bucket, buoys) based on comparisons of the binned but unadjusted SST data with an independent dataset of nighttime marine air temperatures for data through 2010, and adjustments based on buoy SSTs after 2010.

The HadISST is a monthly dataset on a $1° \times 1°$ horizontal grids from 1870 to the present (Rayner et al. 2003). The dataset was constructed using reduced space optimal interpolation applied to SSTs from the Marine Data Bank (mainly ship tracks) and ICOADS, including a blend of in-situ and adjusted satellite-derived SSTs from 1982 onwards. The KAPLAN SST is available on a $5° \times 5°$ horizontal grids and consists of monthly anomalies from 1856 to present. The dataset was constructed from the Met Office database (Parker et al. 1994) through various processing steps including empirical orthogonal functions projection, optimal interpolation, Kalman Filter forecast/analysis, and an optimal smoother (Kaplan et al. 1998). These techniques fill missing data using both spatial patterns derived from the data that exists together with time interpolation.

2.1.3 Air Temperature Dataset

The monthly air temperature shown in Fig. 1 was taken from the University of Delaware dataset version 4.01

Fig. 2 Scatterplot of the normalized monthly GPCC and **a–c** CRU rain gauge precipitation datasets averaged over the (left) Amazon basin, (middle) Congo basin, and (right) Maritime continent for 408 months from January 1981 to December 2014. Panels **d–f**, **g–i**, and **j–l** show the same as **a–c** but for CHIRPS, CMAP, and GPCP satellite/gauge precipitation data sets, respectively. The correlation between the time series pair is indicated in each panel
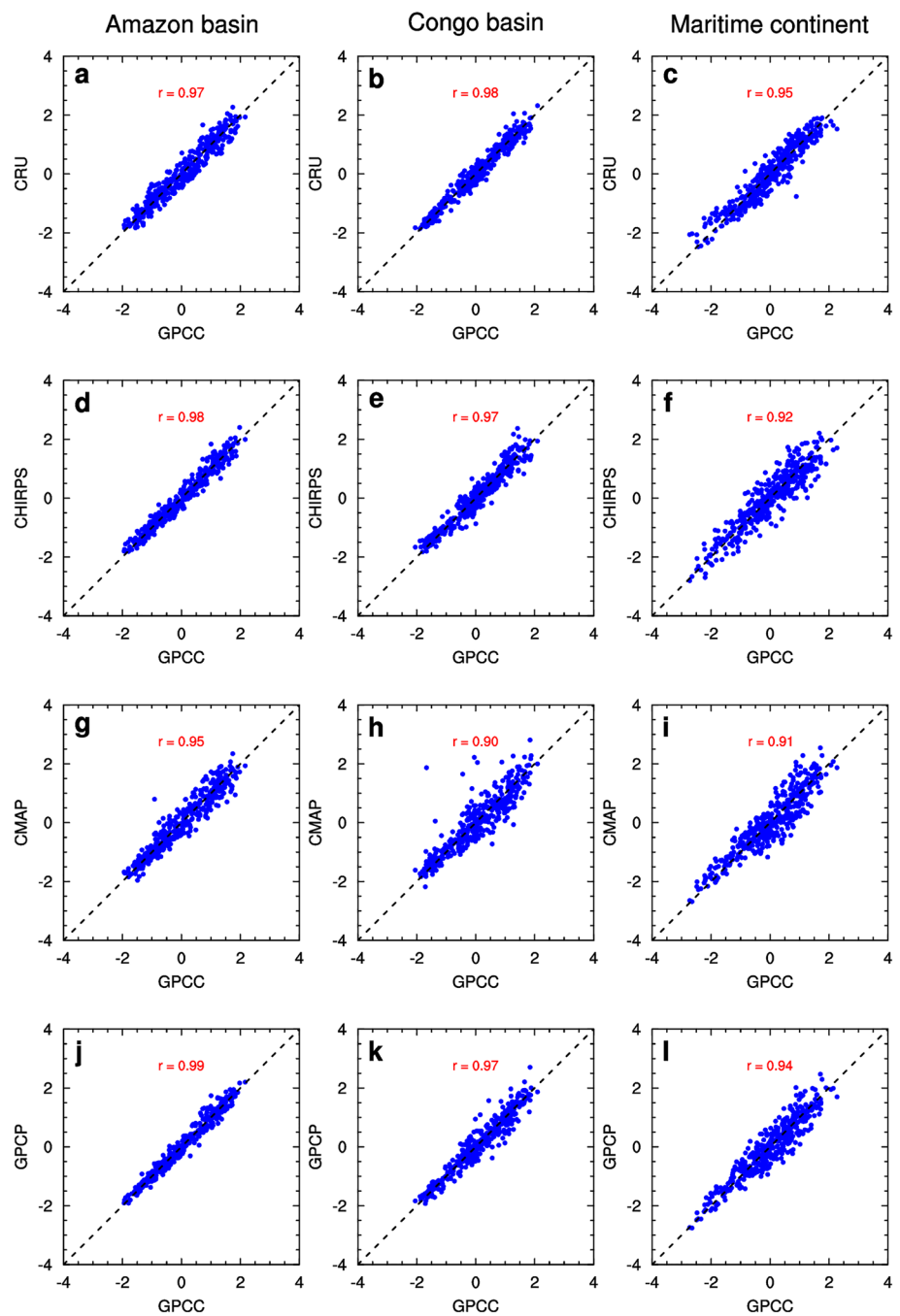
(UDEL) available from 1900 to 2014 (Willmott and Matsuura 1995). It was constructed using numerous stations, both from the Global Historical Climate Network version 2, the Global Surface Summary of Day archive and from the Legates and Willmott (1990) archive. The dataset consists of monthly mean surface air temperatures over the global land surface at a horizontal resolution of 0.5° × 0.5° horizontal grids spacings.

2.1.4 Atmospheric Reanalysis

We use atmospheric fields from version 3 of the Twentieth Century Reanalysis (Slivinski et al. 2019). The reanalysis was constructed using prescribed SST and sea ice distributions and assimilation of surface pressure observations into the National Centre for Environmental Prediction's Global Forecast System version 14.0.1 to generate

a four-dimensional global atmospheric dataset from 1836 to 2015. The system uses an ensemble filter data assimilation method to estimate the state of the global atmosphere 8-times daily. The individual ensemble simulations were performed at a resolution of T254, which corresponds to approximately 60 km at the equator, with a vertical atmospheric resolution of 64 levels from 1000 hPa up to 0.3 hPa. The analysis here is based on the ensemble mean fields that were calculated by averaging over 80 ensemble members at each time step.

2.2 CMIP6 Models

We analyze historical simulations of 24 global climate models taken from the CMIP6 archive (Eyring et al. 2016). The selected models provide the first realisation simulations for the historical simulations of both precipitation and SST. The analysed CMIP6 coupled models, modelling institution name, models' horizontal resolution, and key reference(s) are shown in Table 1. The model's horizontal resolution ranges from 20 km (AWI-CM-1-1-MR, GFDL-ESM4) to 100 km (MPI-ESM1-2-LR) in the ocean, and from 60 km (MRI-ESM2-0) to 250 km (CanESM5) in the atmosphere. We bilinearly remapped the simulated precipitation onto a common 2.5° × 2.5° latitude–longitude grid similar to that of

the GPCC rain gauge dataset, and the SSTs onto a common 1° × 1° latitude–longitude grid consistent with the COBE and HadISST observational datasets.

2.3 Analysis Methods

The analysis covers the common period from 1930 to 2014, shown by dashed vertical lines in Fig. 1e, using the observational data sets and a 24-member multi-model CMIP6 historical ensemble. The anomalies are computed by removing the mean and trends from each month for the entire period prior to subsequent analyses. The only exception is Fig. 1 which shows the climatological-mean precipitation and air temperature as well as the number of rain-gauges per grid-cell. The analysis here is based on the all months such that strongest patterns without the explicit consideration of the seasonality are discussed.

2.3.1 Standardized Precipitation Index

We define precipitation indices calculated as the area-averages of land-only grid point precipitation over the three humid tropical regions (shown by boxes in Fig. 1a), representing the Amazon basin, Congo basin, and Maritime continent. For the CMIP6 models, we first mask out ocean grid

Table 1 Information of the 24 CMIP6 models used to construct the analyzed ensemble

S/N	Model name	Ocean resolution	Atmospheric resolution	Reference(s)
1	ACCESS-CM2	70 km	100 km	Bi et al. (2020), Ziehn et al. (2020)
2	ACCESS-ESM1-5	70 km	100 km	
3	AWI-CM-1–1-MR	20 km	80 km	Sidorenko et al. (2015), Semmler et al. (2020)
4	BCC-CSM2-MR	80 km	100 km	Wu et al. (2019)
5	CanESM5		250 km	Swart et al. (2019)
6	CESM2	60 km	100 km	Danabasoglu et al. (2020)
7	CESM2-WACCM	60 km	100 km	
8	CMCC-CM2-SR5	70 km	100 km	Cherchi et al. (2019)
9	CMCC-ESM2	70 km	100 km	
10	EC-Earth3	70 km	80 km	Döscher et al. (2022)
11	EC-Earth3-Veg-LR	70 km	120 km	
12	EC-Earth3-Veg	70 km	80 km	
13	FGOALS-f3-L	80 km	90 km	He et al. (2020)
14	GFDL-ESM4	20 km	100 km	Dunne et al. (2020)
15	INM-CM5-0	30 km	150 km	Volodin et al. (2017)
16	IPSL-CM6A-LR	70 km	160 km	Boucher et al. (2020)
17	KACE-1–0-G	90 km	140 km	Lee et al. (2020a)
18	MIROC6	80 km	120 km	Tatebe et al. (2019)
19	MPI-ESM1-2-HR	40 km	80 km	Mauritsen al. (2019), Müller et al. (2018)
20	MPI-ESM1-2-LR	100 km	170 km	
21	MRI-ESM2-0	60 km	60 km	Mizuta et al. (2012), Yukimoto et al. (2019)
22	NorESM2-LM	60 km	190 km	Seland et al. (2020)
23	NorESM2-MM	60 km	100 km	
24	TaiESM1	60 km	100 km	Lee et al. (2020b)

points before computing the indices. It is worth pointing out that our approach emphasises the region-wide occurrences of wet and dry conditions. The regional-averaged occurrences of wet and dry conditions over the humid tropics are quantified using the 6-month Standardized Precipitation Index (SPI), a measure of wetness and dryness of various intensities.

The SPI has been widely used for prediction and monitoring of both wet and dry conditions across many regions of the globe (e.g., Mckee et al. 1993; Ajayi and Ilori 2020; Sharma et al. 2021). The SPI is calculated here by fitting a Pearson Type III probability distribution function to the monthly precipitation values, which is then normalized so that the mean SPI for each region and period of interest equals zero (Edwards and McKee 1997; World Meteorological Organization 2012; Khan et al. 2021; Mohammed et al. 2022; Phuong et al. 2022). Positive (negative) values of SPI denote greater (less) than the median precipitation. We use the 6-month SPI, reflecting variations in meteorological and soil moisture conditions. This timescale is relevant for agriculture, which responds to precipitation anomalies on relatively short timescales.

2.3.2 Definition of Extreme Conditions and Composite Analysis

We define extreme wet and dry conditions using the ± 1.5 of the 6-month SPI threshold using regional-averaged precipitation data over the respective humid tropical regions. This approach allows us to focus on the large-scale persistent patterns, rather than specific events at the grid-point level. Our criteria correspond to *very wet* ($+1.5$) and *severely dry* (-1.5) conditions, respectively (World Meteorological Organization 2012). The frequency of occurrence of wet (dry) conditions is determined as the number of months for which the SPI is $+1.5$ (-1.5) and greater (less) divided by the length of the series. These thresholds were used for composite analysis (Xie et al. 2017), by defining the wet pattern (WET) and dry pattern (DRY). Using the SPI as our reference index, we classify field F into an extreme wet conditions set $\mathrm{SPI_{Wet}}$ and extreme dry conditions set $\mathrm{SPI_{dry}}$ as follows:

$$\mathrm{WET} = \frac{\Sigma \chi \mathrm{SPI_{wet}}\left(\mathrm{SPI}_i\right) \cdot F_i}{\Sigma \chi \mathrm{SPI_{wet}}\left(\mathrm{SPI}_i\right)}, \mathrm{DRY} = \frac{\Sigma \chi \mathrm{SPI_{dry}}\left(\mathrm{SPI}_i\right) \cdot F_i}{\Sigma \chi \mathrm{SPI_{dry}}\left(\mathrm{SPI}_i\right)} \quad (1)$$

where, $\mathrm{SPI_i}$ and F_i are the ith time point of *SPI* and *F*, respectively, wet (dry) is defined by the $+1.5$ (-1.5) threshold and

$$\chi\left(\mathrm{SPI_{wet}}\right) = \begin{cases} 1, \mathrm{SPI}_i \in \mathrm{SPI_{wet}} \\ 0, \mathrm{SPI}_i \notin \mathrm{SPI_{wet}} \end{cases}, \chi\left(\mathrm{SPI_{dry}}\right) = \begin{cases} 1, \mathrm{SPI}_i \in \mathrm{SPI_{dry}} \\ 0, \mathrm{SPI}_i \notin \mathrm{SPI_{dry}} \end{cases} \quad (2)$$

The statistical significance is determined using a two-tailed *t*-test, and the 95% confidence interval marked. For the CMIP6 patterns, the composite maps were first computed for the individual models and then averaged over the 24 ensemble members.

2.3.3 Computation of Velocity Potential, Divergence, and Diabatic Heating

Here, we show the winds and diabatic heating anomalies through which the SST anomalies (see later on Fig. 6a–f and corresponding discussions) can be linked to the extreme conditions over the humid tropics. According to Helmholtz's theorem, the total circulation $\mathbf{u} = (u,v)$ can be separated into two components, namely the divergent ("vorticity free") and rotational ("divergence free") wind components:

$$u = -\Delta \chi + k \times \Delta \psi \quad (3)$$

where χ is the velocity potential function; ψ is the streamfunction, and k is a unit vector directed vertically. χ is obtained from $\Delta^2 \chi = \delta$; where δ is the divergence ($\partial u/\partial x + \partial v/\partial y$), which represents the spreading out of the wind flow. Here, we apply the Helmholtz decomposition to the horizontal velocity from the daily reanalysis to determine the upper-level (200 hPa) and near-surface (850 hPa) divergent winds and velocity potential fields. The daily fields are then averaged to monthly fields and linked to the extreme wet and dry conditions over the humid tropics using composite analysis.

Diabatic heating denotes the combined consequence of radiative fluxes, phase changes of water substance, and turbulent flux of sensible heat from the Earth's surface. It indicates atmospheric convection and is strongly correlated with SST variability over the tropics (Ling and Zhang 2013; Stechmann and Ogrosky 2014; Nnamchi et al. 2021). Here, we compute the diabatic heating using the apparent heat source (Q_1) as a residual of the thermodynamic equation (Yanai et al. 1973):

$$Q_1 = \frac{\partial T}{\partial t} - \left(\omega \sigma - \frac{u \partial T}{\partial x} + \frac{v \partial T}{\partial y} \right) \quad (4)$$

where T denotes the air temperature, ω the vertical pressure velocity, $\sigma = (RT/C_p p) - (\partial T/\partial p)$ is the static stability, q the specific humidity, R the gas constant ($R = 287$ Jkg^{-1} K^{-1}), p the air pressure and C_p the specific heat capacity at constant pressure ($C_p = 1004.64$ J kg^{-1} K^{-1}). Differential operators, x, y, and t are along zonal and meridional directions, and time, respectively. The Q_1 was first computed for all atmospheric levels using daily data and then averaged to monthly data for composite analysis.

3 Results

3.1 The Observations of Extreme Wet and Dry Conditions

3.1.1 Occurrences of the Conditions

Figure 3 displays the 6-month SPI averaged over the Amazon basin, Congo basin, and Maritime continent, respectively. Overall, the 6-month SPI exhibits strong interannual variations and potentially some decadal modulations in all three regions (Fig. 3a–c). To better characterize the SPI,

we quantify the occurrences of very wet (severe excess rainfall) conditions and severely dry (severe rainfall deficits) conditions using the ± 1.5 threshold, which are marked by dashed horizontal lines in Fig. 3a–c.

Both wet and dry conditions occur throughout the year (Fig. 3d–f), although the occurrence of extreme wet conditions is smallest during the austral summer in the Congo basin (Fig. 3e). Generally speaking, the occurrences of dry conditions exceed those of the wet conditions continuously from November to May at the Amazon basin (Fig. 3d) and November to January at the Congo basin (Fig. 3e). This is in line with reports of recent long drying trends in the Congo basin (Nicholson et al. 2022; Cook et al. 2020) and
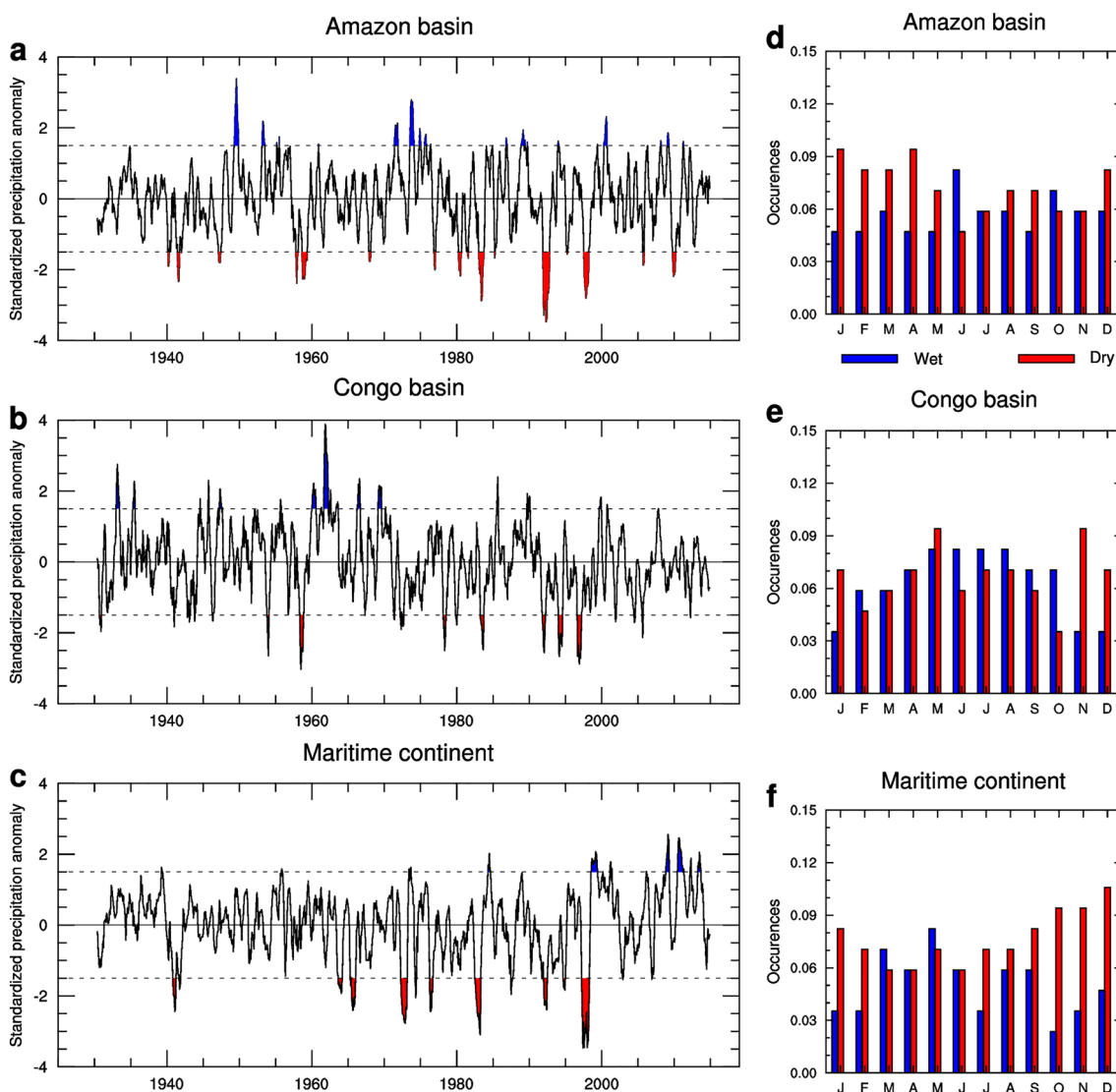
Fig. 3 Six-month standardized precipitation index (SPI) averaged over the **a** Amazon basin, **b** Congo basin, and **c** Maritime continent. The dashed horizontal lines (± 1.30) delineate the severely wet ($+1.30$) and severely dry (-1.30) episodes. Frequency of occur-

rences of the severely wet and severely dry conditions in different months are shown for **d** the Amazon basin, **e** the Congo basin, and **f** the Maritime continent

the recent Amazon basin extreme droughts conditions in 1998, 2006, 2010 (see also red fills in Fig. 3a; Marengo et al. 2011). For the Maritime continent, which exhibits the highest occurrences of dry conditions of all three regions, the dry conditions exceed wet conditions from July to February (Fig. 3f). This is consistent with the persistence of dry extreme conditions (denoted by red fills in Fig. 3c) compared to the extreme wet conditions (represented by the blue fills in Fig. 3c).

3.1.2 The Characteristic Precipitation Anomalies

As expected, the typical extreme wet condition in each humid tropical region is characterized by excessive precipitation over the humid tropics in the GPCC observational dataset (Fig. 4). The extreme wet condition over the Amazon is associated with reduced precipitation over the La Plata Basin from Brazil to Argentina, forming a dipole pattern over South America (Fig. 4a). Strikingly, there is also increased precipitation over the Maritime continent as well as southern Africa. The precipitation patterns during extreme wet and dry conditions over the Maritime continent closely reproduce the patterns associated with the Amazon. These patterns of precipitation anomalies are reversed during extreme dry conditions, which are also characterized by dry conditions over the Maritime continent and southern

Africa but greatly enhanced precipitation over the La Plata Basin (Fig. 4d).

The extreme wet (dry) conditions over the Congo basin are associated with reduced (increased) precipitation over the La Plata Basin (Fig. 4b, e), while over the Maritime continent, it is associated with extreme wet (dry) precipitation (Fig. 4b, e). Although the reanalysis bears some resemblance to the GPCC gauge-based data over lands generally (Fig. 4g–l), the Congo Basin, as well as the related patterns over the La Plata Basin, are poorly represented in the reanalysis (Fig. 4h, k).

## 3.2 Multiple Oceanic Drivers of the Wet and Dry Conditions

3.2.1 Related SST Variability in the Tropical Pacific, Indian, and Atlantic Oceans

The simultaneous SST variability over the tropical Pacific, Indian, and Atlantic Oceans associated with the humid tropics' conditions computed obtained from the various datasets (COBE, ERSST, HadISST, and KAPLAN) are shown in Fig. 5. Strikingly, the extreme wet (dry) conditions are consistently linked to cold (warm) SST anomalies in the tropical Pacific reminiscent of La Niña (El Niño), representing the negative (positive) phase of El
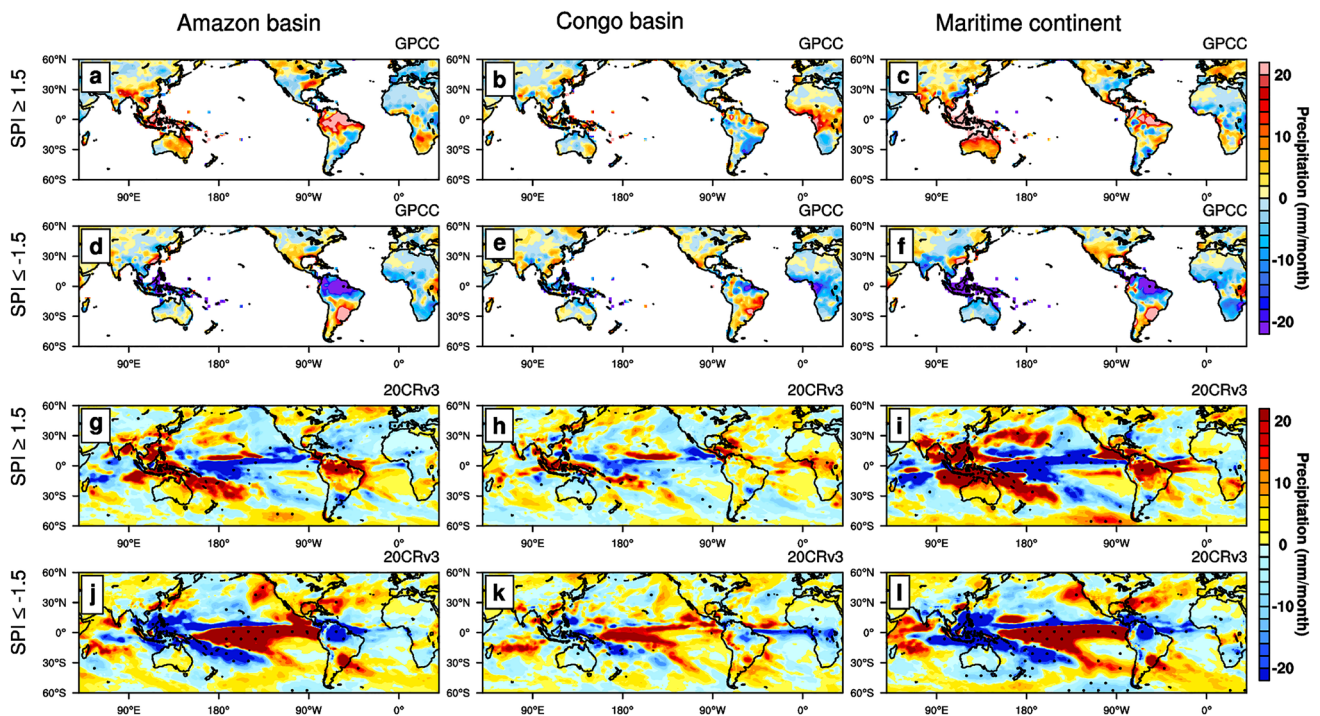
Fig. 4 Composite patterns of **a–f** GPCC precipitation and **g–l** reanalysis precipitation anomalies associated with wet (SPI ≥ 1.5) and dry (SPI ≤ − 1.5) conditions for Amazon basin (left panels), Congo basin (middle panels), and Maritime continent (right panels). Stipples denote statistical significance at the 95% confidence level
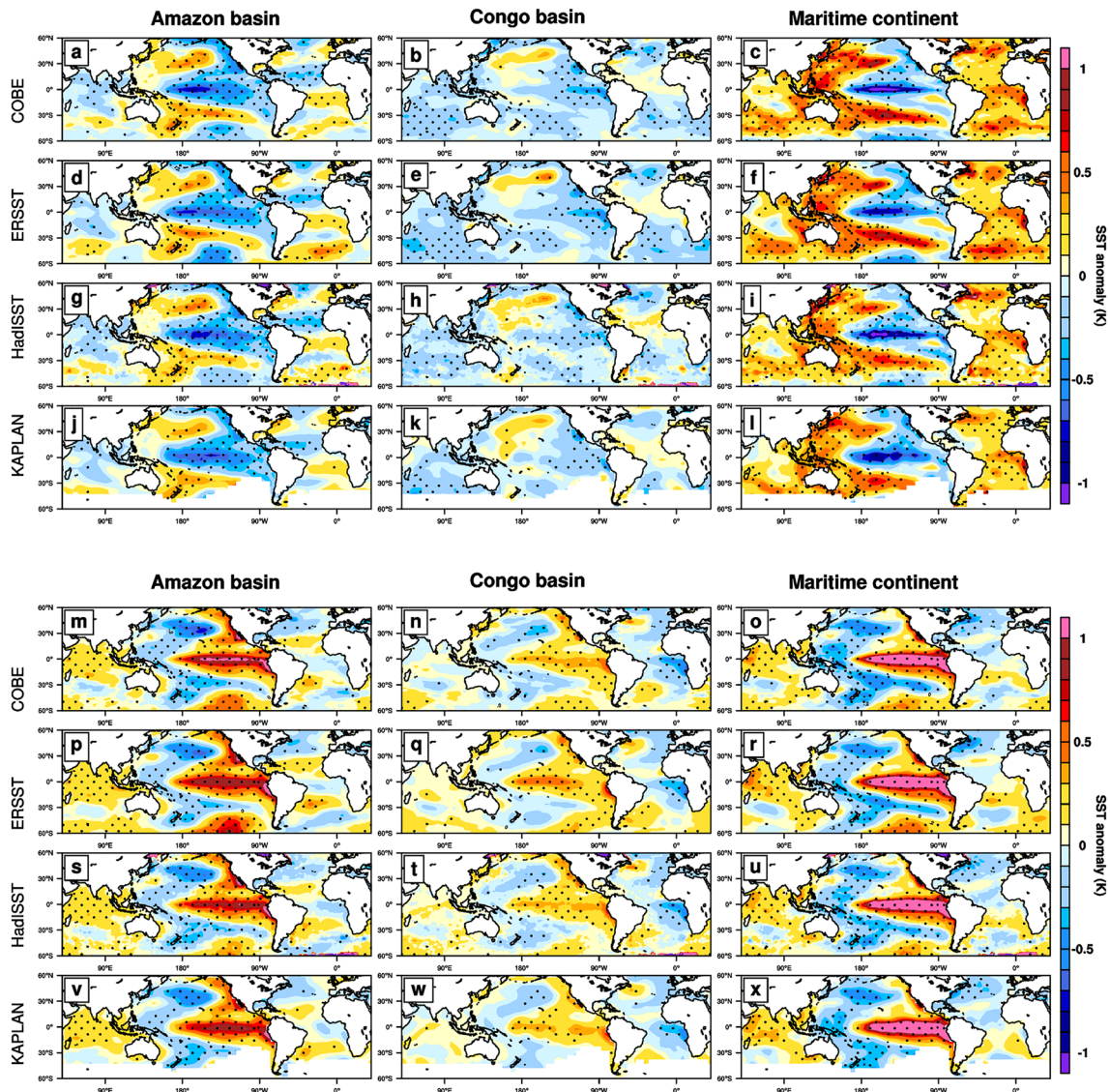
Fig. 5 Composite patterns of SST anomalies associated with extreme wet conditions (**a–l**) and extreme dry conditions (**m–x**) over the Amazon basin (left panels), Congo basin (middle panels), and Maritime continent (right panels) based on the multiple datasets indicated beside the leftmost panels. The stipples denote statistical significance at the 95% confidence level

Niño Southern Oscillation (ENSO). It must be pointed out that while the extreme wet conditions over the Amazon and Maritime continent are associated with Central Pacific-type (CP) La Niña SST anomalies, the dry conditions in these regions are linked to Eastern Pacific (EP) El Niño SST anomalies. Furthermore, the magnitudes of the SST anomalies differ slightly across the four datasets, and markedly among the conditions (wet versus dry) over the regions. The link to ENSO-type SST anomalies are overall least robust for the Congo basin, and are shown on the middle panels of Fig. 5. Specifically, the extreme wet conditions over the Congo basin which are associated with cold SST anomalies in the eastern tropical Pacific in HadISST and KAPLAN (Fig. 5h, k) but a more clearly

defined albeit weak La Niña pattern in the COBE and ERSST datasets (Fig. 5b,e).

In all cases, there are significant SST anomalies in the tropical Indian and Atlantic Oceans, which points to the roles of ocean basins interaction for the humid tropics (Latif and Barnett 1995; Cai et al. 2019). However, the impacts of SST anomalies in these basins are quite different for the different humid tropical regions. The extreme wet (dry) conditions over the Amazon basin are associated with homogeneous cold (warm) SST anomalies in the tropical Indian Ocean. However, it is rather unclear if this pattern is related to the Indian Ocean Basin wide mode (Klein et al. 1999; Huang and Kinter 2002; Schott et al. 2009; Huang et al. 2019), which is is mainly forced by ENSO (e.g., Klein et al. 1999;

Ding et al. 2022). These tropical Indian Ocean homogenous SST anomalies are overall more robust in COBE and Had-ISST (Fig. 5a, g), both of which are comparatively higher resolution at a $1° \times 1°$ horizontal latitude–longitude grids, during the Amazon extreme wet conditions. In the Atlantic, there is an ADO pattern characterized by meridional bands of alternating warm and cold SST anomalies (left panels of Fig. 5; Xie and Tanimoto 1998; Nnamchi et al. 2023). The Amazon wet conditions are associated with the colder-than-normal SST anomalies over the tropical North Atlantic and warmer-than-normal SST anomalies over the tropical South Atlantic, representing the negative of the AMM. On the other hand, the Amazon dry conditions are associated with the positive phase of the AMM.

The extreme wet conditions over the Congo basin are linked to homogeneous cold SST anomalies over the Indian Ocean (Fig. 5b, e, h, k). Cold SST anomalies in the tropical Indian Ocean drive upper tropospheric convergence and divergence over Central Africa (Bader and Latif 2003), leading to enhanced convection there as suggested by the diabatic heating anomalies (Fig. 5b, h, n). However, the Indian Ocean SST anomalies during the Congo basin extreme dry conditions are not statistically significant (Fig. 5n, q, t, w). This lack of symmetry is also seen in the Atlantic SST patterns associated with the Congo basin between the wet and dry extremes. The extreme dry conditions are characterised by Atlantic Niña-like cold SST anomalies, that is, stronger-than-normal cooling of the Atlantic cold tongue region (Fig. 5n, q, t, w). Hua et al. (2016) reported that the drying trend over the Congo basin has been driven by SSTs changes over the tropical Atlantic and in the Indo-Pacific sector, while Cook et al. (2020) associated the extreme dry conditions over the Congo basin with surface warming. The SST anomalies in the Atlantic cold tongue region are neutral, i.e., not different from zero during the extreme wet conditions over the Congo basin (Fig. 5b, e, h, k). The extreme wet conditions over the Congo basin are linked to weak EP-type La Niña, cold SST anomalies over the Indian Ocean or generally cold SST anomalies across the global tropical oceans depending on the dataset. Nicholson et al. (2022) examined wet versus dry conditions in the region, although using different methods than the present study, they linked the wetter conditions to changes to pacific SST and tropical Walker circulation.

For the Maritime continent, both extreme wet and dry episodes are associated with homogeneous warm SST anomalies in the tropical Indian Ocean, with opposite phases of La Niña (wet conditions) and El Niño (dry conditions) in the Pacific (right panels of Fig. 5). The absolute magnitudes of the associated El Niño clearly exceed those of the La Niña SST anomalies. There are also widespread warmer-than-normal SST anomalies across the Atlantic which appear as the Atlantic Niño over the tropics during the extreme wet

conditions over the Maritime continent. However, the Atlantic Niño region SST anomalies are not different from zero during extreme dry conditions, pointing to a lack of symmetry in the Atlantic link to the wet and dry conditions over the Maritime continent.

Overall, one striking feature of Fig. 5 is that the Pacific and Indian Oceans exhibit consistent SST anomalies associated with the wet and dry conditions across the humid tropics. While the Pacific exhibits ENSO-like patterns, the Indian Ocean exhibits homogeneous patterns. In contrast, however, the related Atlantic SST anomalies are generally inconsistent. In other words, the pattern of SST anomalies associated with the extreme conditions over the Amazon, Congo basin and Maritime continent are markedly different. Furthermore, except for the ADO-Amazon connection shown on the left panels of Fig. 5, the SST anomalies are also non-symmetrical between the extreme wet and dry conditions. Finally, generally warm SST anomalies across the Atlantic are associated with the Atlantic Niño during extreme wet conditions over the Maritime continent (Fig. 5c, f, i, l). In contrast, the Atlantic Niña pattern associated with extreme dry conditions over the Congo basin is confined to the Atlantic cold tongue region (Fig. 5n, q, t, w).

3.2.2 Underling Atmospheric Convection and Circulation Patterns

During extreme wet conditions over the humid tropics, the La Niña-type SST anomalies over the eastern equatorial Pacific (Fig. 5a–l) can be linked to intensified southeasterly trade winds (Bjerknes 1969; Cai et al. 2020). This is accompanied by increased low-level divergence, indicated by the negative velocity potential anomalies and anomalous divergent wind vectors, in the climatological-mean sinking branch of the Walker Circulation over the eastern equatorial Pacific (Fig. 6a–c). These are associated with an opposite pattern, implying anomalous intensification of the mean convection and low-level convergence over the Pacific Warm Pool-Maritime continent complex. The anomalous divergent winds flow away from regions of negative velocity potential anomalies and converge over the regions with positive velocity potential anomalies. The anomalous low-level convergence fields can be linked to upper-level divergence and enhanced deep convection over the Warm Pool-Maritime continent complex which drives the atmospheric circulation anomalies (Fig. 6g–i). Enhanced convection is shown by elevated diabatic heating anomalies (Fig. 6m–o) and these are collocated with increased precipitation over the respective humid tropical regions (see Fig. 4).

As El Niño-type SST anomalies prevail during extreme dry conditions over the humid tropics (Fig. 5m–x), the above diabatic heating and atmospheric circulation anomalies are reversed (Fig. 6d–f, j–l, p–r). Specifically, upper-level
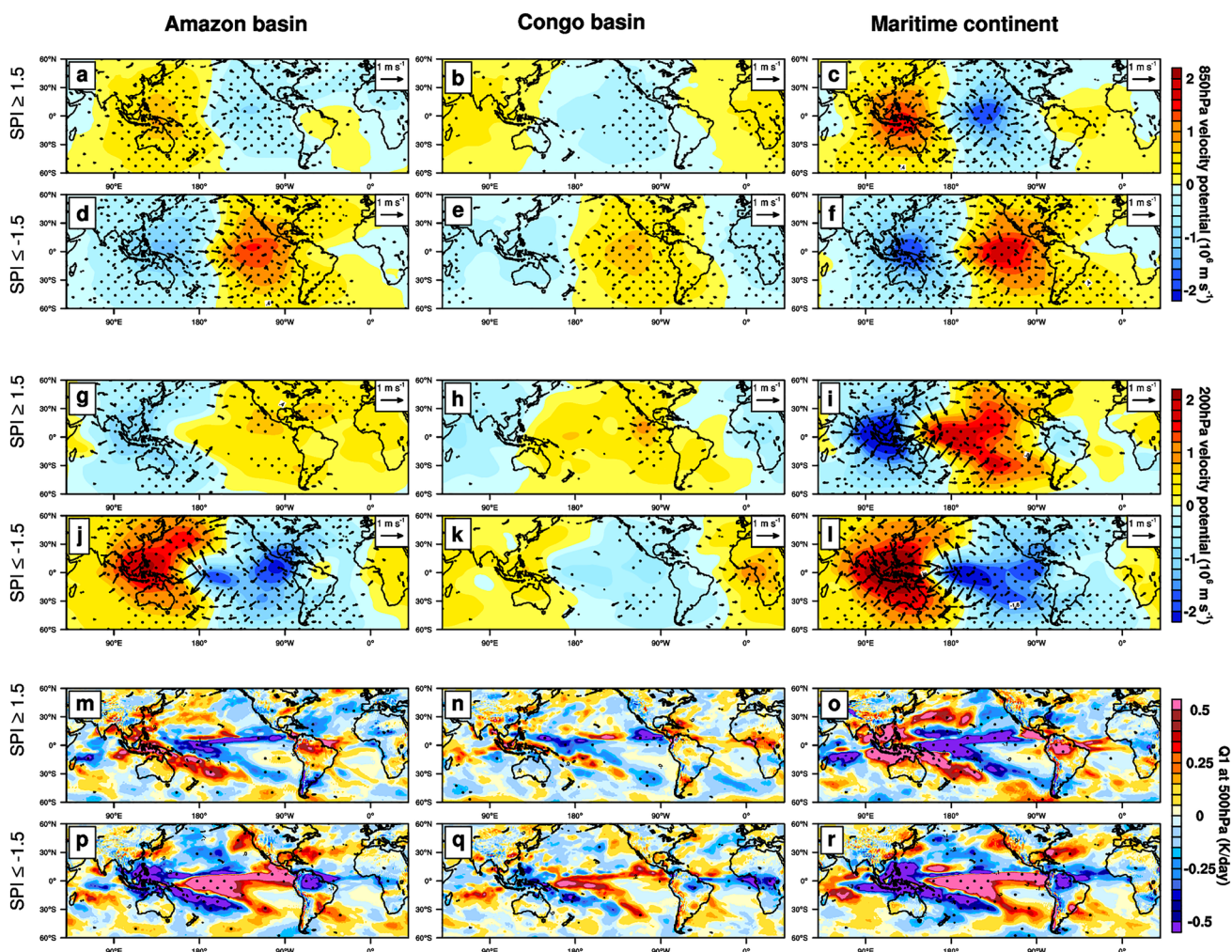
Fig. 6 The shading shows the composite patterns of **a–l** 850 and 200 hPa velocity potential anomalies, and **m–r** 500 hPa diabatic heating anomalies associated with extreme wet (SPI ≥ 1.5) and extreme dry (SPI ≤ − 1.5) conditions over the Amazon basin (left panels), Congo basin (middle panels), and Maritime continent (right panels). The stipples denote statistical significance at the 95% confidence level. The arrows in **a–l** show the divergent wind anomalies, and only statistically significant vectors are plotted

convergence is accompanied by low-level divergence leading to reduced diabatic heating over the Warm Pool-Maritime continent complex. On the other hand, upper-level divergence anomalies that are associated with low-level convergence and increased diabatic heating prevail over the eastern equatorial Pacific.

These analyses ultimately point to the strengthening and weakening of the mean Walker Circulation especially in the Indo-Pacific region that is associated with extreme dry conditions over the humid tropics. The La Niña-type SST pattern over the tropical Pacific drives a stronger-than-average Walker Circulation leading to extreme wet conditions, whereas the El Niño-type pattern is linked to weaker-than-average Walker Circulation and extreme dry conditions, over the humid tropics. The impacts of the Pacific are essentially modulated by the Indian and Atlantic Oceans. Specifically,

the extremes over the Congo basin, which exhibits the least robustness of the ENSO pattern in the Pacific, appear to be mostly influenced by the SST over the Indian and Atlantic Oceans as well as diabatic heating anomalies over the Atlantic–African–Indian region.

3.3 The Extreme Wet and Dry Conditions in CMIP6 Historical Ensemble

3.3.1 Simulated Frequencies and Magnitudes

Next, we investigate how well the current generation of state-of-the-art climate models represent the observed occurrences and magnitudes of extreme wet and dry conditions over the humid tropics in the 24-member multi-model CMIP6 historical ensemble (Fig. 7). Generally
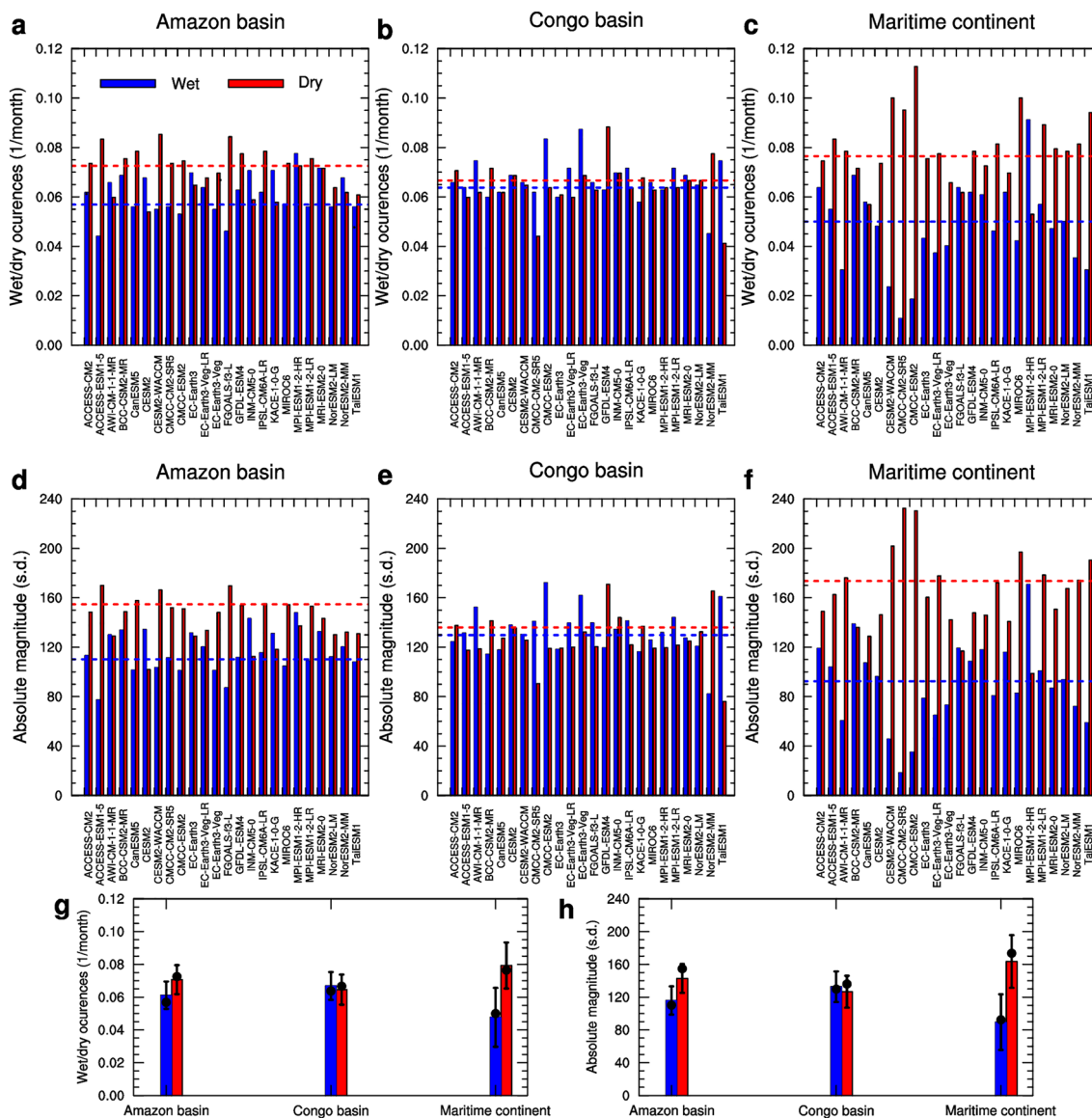
Fig. 7 Frequencies and absolute magnitudes of the wet/dry conditions in **a**, **d** Amazon basin, **b**, **e** Congo basin, and **c**, **f** maritime continent in CMIP6 historical ensemble for the 1930–2014 period. Dashed line in each panel represents the observed occurrences. The multi-model means and 95% confidence limit (determined as ±standard devia-tions) are shown by error bars for the **g** occurrences and **h** absolute intensity. The blue (red) bars denote wet (dry) conditions in all panels. In **g** and **h**, there is a significant difference between the wet and dry conditions when the error bar associated with the blue bar is out-side the vertical segment of the error bar associated with the red bar

speaking, majority of models tend to simulate higher frequencies and magnitudes of extreme dry conditions compared to the wet conditions, especially over the Maritime continent and Amazon basin. One exception, however, is the MPI-ESM1-2-HR which clearly depicts a larger frequency and magnitude of extreme wet conditions over the Maritime continent. In contrast, models such as CESM2, CESM2-WACCM, CMCC-CM2-SR5, CMCC-ESM2, and TaiESM1 simulated small (large) occurrences and magnitudes of extreme wet (dry) conditions over the Maritime continent (Fig. 7c, f).

For the Amazon basin (Fig. 7a), most models simulate a larger frequency and magnitude of extreme dry conditions compared to extreme wet conditions, but the differences are not as dramatic as the Maritime continent. For the Congo basin, there is somewhat of a balance between the extreme wet and dry conditions, and this is consistent with a small spread between these conditions in observations (Fig. 7b, e).

The multi-model ensemble means, and confidence limits (Fig. 7g, h) show that while their frequencies of occurrence are on the margin, the magnitude of extreme dry conditions is larger than that of the extreme wet conditions for the

Maritime continent. The extreme wet and dry conditions exhibit similar occurrences and magnitudes over the Congo basin. For the Amazon basin, the extreme dry conditions display larger mean frequency and magnitude, but these are not statistically different from those of the extreme wet conditions.

### 3.3.2 The Simulated Precipitation and Related SST Anomalies

Consistent with observations, our ensemble-mean of 24 CMIP6 models clearly shows regional-scale increases (decreases) in precipitation during the extreme wet (dry) conditions over the humid tropics (Fig. 8a–f). Furthermore, the precipitation anomalies associated with extreme conditions are remarkably similar for the Amazon basin as well as Maritime continent and are in agreement with the observations. These are characterized by negative (positive) precipitation anomalies implying reduced (increased) diabatic heating over the equatorial Pacific during extreme wet (dry) conditions. However, the Congo Basin extreme conditions are associated with a reversal of the precipitation anomalies over the equatorial Pacific, and this is inconsistent with observations.

The composite SST anomalies associated with the extreme wet and dry conditions over the humid tropics are shown in Fig. 8g–l. The extreme conditions over the

Amazon basin and Maritime continent can be linked to ENSO-like SST anomalies over the tropical Pacific. As expected, the extreme wet conditions are accompanied by CP La Niña-type SST anomalies. The extreme dry conditions are also associated with CP El Niño-type SST anomalies (although more to the east than the simulated La Niña), which is inconsistent with observations. Overall, the simulated maximum (absolute) SST anomalies are confined to narrower north–south bands compared to observations. The extreme wet conditions over the Congo basin is associated with Atlantic Niño SST variability whereas the observed Pacific link is not seen in the CMIP6 ensemble.

Figure 8 clearly shows the inability of the CMIP6 ensemble to reproduce the observed Atlantic SST patterns associated with the extreme hydroclimatic conditions across the humid tropics as well as the relationship between the extreme conditions over the Congo basin and SST anomalies.

The mean-sate biases in the eastern tropical Atlantic that link the Benguela and Atlantic Niño regions constitute a long-standing problem (Davey et al. 2002; Richter and Xie 2008; Richter et al. 2014; Xu et al. 2014; Milinski et al. 2016; Richter and Tokinaga 2020). The mean SST biases (Fig. 9a) can be linked to wet biases in precipitation extending over the tropical Atlantic and the Congo basin (Fig. 9b). This implies a biased representation of the main precipitation band, due to a southerly location of the mean ITCZ, and is connected to a too warm SST bias. Thus, the extreme wet
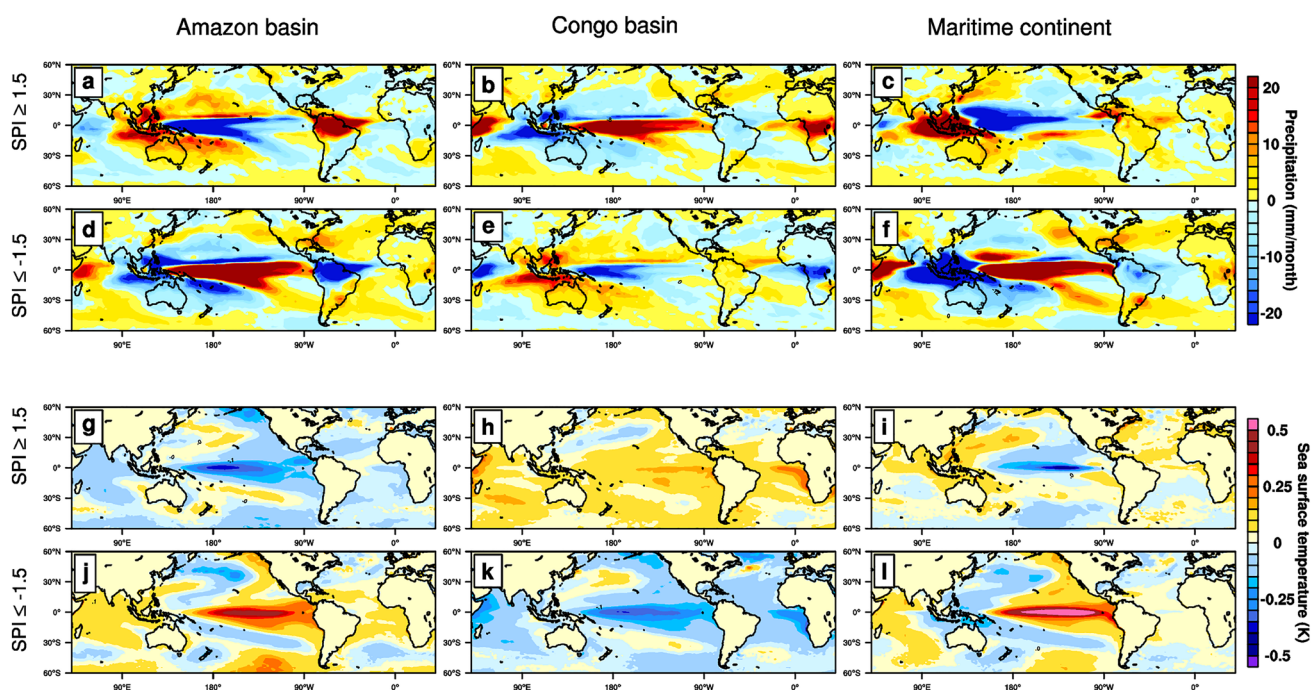
Fig. 8 CMIP6 historical ensemble-mean composite patterns of **a–f** precipitation and **g–l** sea surface temperature (SST) anomalies associated with wet (SPI ≥ 1.5) and dry (SPI ≤ − 1.5) conditions over (i)

Amazon basin (left panels), (ii) Congo basin (middle panels), and (iii) Maritime continent (right panels) for the 1930–2014 period
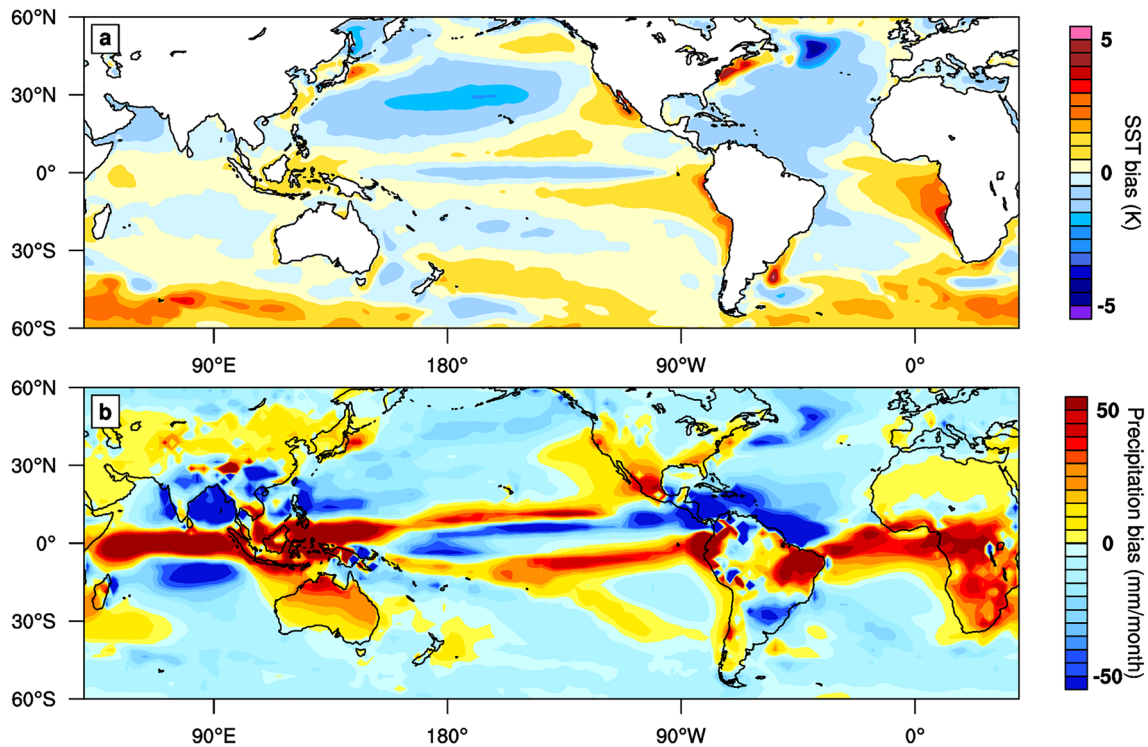
Fig. 9 24 CMIP6 multi-model ensemble mean state biases in **a** SST and **b** precipitation for the 1930–2014 period. The biases are defined as the CMIP6 ensemble-mean *minus* observations. The mean state biases for SST (precipitation) are calculated with respect to the Had-ISST (20CR reanalysis)

(dry) conditions over the Congo basin are tied to the Atlantic Niño (Niña) pattern (Fig. 8) in the CMIP6 ensemble, which is inconsistent with observations (Fig. 5). There are also biases in the tropical Pacific and Indian Oceans (Fig. 9), particularly the double-ITCZ bias in the Pacific (Mechoso et al. 1995; De Szoeke and Xie 2008; Adam et al. 2018; Tian and Dong 2020). Nonetheless, the gross features of the observed Indo-Pacific SSTs associated with the Amazon and Maritime continent are fairly well reproduced in the CMIP6 ensemble, despite the biases. Overall, these results suggest that accurately capturing the relationship between the precipitation extreme conditions and large-scale atmospheric circulations associated with SSTs pattern changes is critical for skillful climate predictions over humid tropics, to produce more reliable climate predictions to inform policies.

4 Discussions, Limitations, and Outlook

4.1 Discussions

Consistent with the prevailing ENSO-centric view of tropical climate variability (e.g., Cai et al. 2019), this analysis shows that the extreme wet (dry) conditions across the humid tropics are consistently linked to La Niña (El Niño) type SST anomalies over the tropical Pacific—representing the negative (positive) phase of ENSO. The associated upper-level divergence (convergence) drives enhanced (diminished) low-level convection over the Pacific Warm Pool-Maritime continent complex and is linked to decreased (increased) low-level convection over the eastern equatorial Pacific. Ultimately, these patterns imply fluctuations in the strength of the mean Walker Circulation, leading to extreme wet conditions over the Amazon, and Maritime continent, and to a lesser extent over the Congo basin.

Beyond ENSO, however, it must be stressed that multiple oceanic influences including those from Indian and Atlantic Oceans are indeed linked to the extreme conditions over the humid tropics. These influences are expressed as homogeneous warm or cold SST variability over the tropical Indian Ocean (Klein et al. 1999; Schott et al. 2009; Huang et al. 2019), the Atlantic Niño (Zebiak 1993; Lübbecke et al. 2018; Foltz et al. 2019), the ADO (Xie and Tanimoto 1998; Nnamchi et al. 2023). The ADO extends beyond the tropics, with alternative bands of cold and warm SST anomalies from the South Atlantic to the subpolar regions of the North Atlantic, and is dominated by 10–15 year periodicity. Thus, the connection of the extreme wet and dry conditions over the humid tropics to the ADO-like pattern we show

in this study raises the question of low-frequency modulation of these conditions and the roles of forcing from the extra-tropics.

For instance, the low-frequency rainfall variability over the Congo basin is correlated with multiple climate indices such as those of the North Atlantic Oscillation, the Atlantic multidecadal oscillation, and the Pacific decadal oscillation (Lüdecke, et al. 2021). Previous studies have shown low-frequency hydroclimate variability of rainfall over the Amazon (Marengo 2004; Wang et al. 2011; Fernandes et al. 2015), linked to a cross-equatorial SST gradient reminiscent of the regional expression of the ADO in the tropical Atlantic (Fernandes et al. 2015). The Maritime continent also exhibits strong decadal variability, which affects its predictability, with the precipitation being more predictable in decades dominated by El Niño and less predictable in decades dominated by La Niña (Li et al. 2022). Compared to La Niña, El Niño drives stronger ocean–atmosphere interactions across the tropics, leading to stronger precipitation variability and predictability over the Maritime continent (Lee and Lo 2021; Li et al. 2022; Xiao et al. 2022).

The most striking feature in our analysis is that while the Pacific and Indian Oceans exhibit consistent SST anomalies linked to the wet and dry conditions across the humid tropics, the Atlantic impacts are quite inconsistent, and non-symmetrical. An ensemble-mean of 24 CMIP6 models fails to reproduce these patterns, representing a key challenge for seasonal climate prediction and climate change projections over the humid tropical regions.

The CMIP6 ensemble reproduces the observed La Niña (El Niño) link to extreme wet (dry) conditions over the Amazon and Maritime continent, although the simulated SST anomalies are smaller than the observations. In contrast, the observed signs of SST anomalies in the tropical Pacific and Indian Oceans associated with the Congo basin are reversed in the CMIP6 ensemble. The modelled occurrences of extreme wet and dry conditions over the Congo basin are tied to the Atlantic Niño variability. This strong connection can be explained by warm SST biases over the Benguela-Atlantic Niño complex (Davey et al. 2002; Richter and Tokinaga 2020; Farneti et al. 2022) and wet biases over the tropical Atlantic extending over the Congo basin. There are also mean state biases in the Pacific and Indian Oceans such as the double ITCZ bias in the tropical Pacific (Mechoso et al. 1995; Tian and Dong 2020). Nonetheless, the simulated connections of the Amazon and Maritime continent to the Indo-Pacific variability are, nonetheless, generally more realistic in comparison to the Atlantic–Congo basin connection. Thus, model improvements for the humid tropics (particularly the Congo basin) will require a focused effort to correctly represent the region's observed large-scale teleconnections to oceanic and atmospheric variability in the Pacific, Indian, and Atlantic Oceans.

4.2 Limitations and Outlook

The composite analyses are presented here based on simultaneous monthly data for the period 1930–2014. These results, therefore, represent the averages over an 85-year long time span during which phase relationships between the extreme wet and dry conditions, and potential forcing from the different ocean basins may have undergone phase shifts. Indeed, all three humid tropical regions analyzed show some decadal modulations (Fig. 3a–c) that were not further investigated here. Moreover some relationships can only be detected when seasonality and time lags are taken into consideration. The representation of precipitation variability over humid tropics, including the roles of seasonality, and external forcing, can vary substantially across the CMIP6 models (Eyring et al. 2021; Chiang et al. 2021; Baker and Spracklen 2022). Questions such as how these considerations may affect the patterns described here, as well as the mechanisms underlying the inconsistent and non-symmetric Atlantic impacts, need to be investigated in further studies.

5 Summary and Policy Implications

5.1 Summary and Concluding Remarks

- The 6-month SPI is associated with coherent wet and dry patterns over the humid tropical regions (Amazon basin, Congo basin, and Maritime continent), with strong interannual variability and some potentially decadal modulations. The occurrences of extreme dry conditions (SPI $\lesssim -1.5$) generally exceed those of the wet conditions (SPI $\gtrsim +1.5$) over all three regions.

- The observed extreme wet conditions are consistently linked to La Niña-type patterns, whereas the extreme dry episodes are associated with El Niño-type patterns in the tropical Pacific. Specifically, the Amazon and Maritime continent wet (dry) conditions are associated with CP (EP) La Niña (El Niño) SST anomalies. The Congo basin extreme conditions tend to be associated with EP patterns. The amplitudes of the La Niña/El Niño SST anomalies differ markedly among the regions, being generally small and uncertain in some datasets for the Congo basin.

- Beyond the La Niña/El Niño, all regions are also associated with significant SST anomalies in the tropical Indian and Atlantic Oceans, pointing to the important roles of ocean basins interactions. The extreme wet (dry) conditions over the Amazon are associated with homogeneous cold (warm) SST anomalies in the tropical Indian Ocean and negative (positive) ADO phases, whereas the warm tropical Indian Ocean pattern is linked to both the wet and dry conditions over the Maritime continent. Strik-

ingly, while the Pacific and Indian Oceans exhibit consistent SST anomalies linked to the wet and dry conditions across the humid tropics, the Atlantic impacts are quite inconsistent, and non-symmetrical.

- The Congo basin and Maritime continent exhibit non-symmetrical response to the tropical Indian and Atlantic Oceans. While the extreme wet conditions over the Congo basin are linked to cold tropical Indian Ocean patterns, the SST anomalies during the extreme dry conditions are not different from zero. The extreme wet conditions over the Maritime continent are associated with the Atlantic Niño but no significant SST anomalies in the Atlantic Niño region during the dry conditions.

- The extreme wet and dry conditions over the humid tropics are linked to the SST anomalies through fluctuations of the mean Walker Circulation especially in the Indo-Pacific region particularly over the Amazon basin and Maritime continent, modulated by the Indian and Atlantic Oceans. The Congo basin exhibits smallest connection to large-scale ocean–atmosphere in the tropical Pacific and is potentially mostly influenced by the SST in the Indian and Atlantic Oceans as well as diabatic heating over the Atlantic-African-Indian region.

- Consistent with observations, the extreme wet conditions over the Amazon basin and Maritime continent are linked to CP La Niña-type SST anomalies in an ensemble of 24 CMIP6 models. The extreme dry episodes are also associated with CP El Niño-type SST anomalies, which is inconsistent with observations. The extreme wet/dry conditions over the Congo basin are associated with Atlantic Niño/Niña variability whereas the observed Pacific links are not seen in the CMIP6 multi-model ensemble. The CMIP6 ensemble fails to simulate the observed Atlantic SST anomalies associated with the extreme conditions over the humid tropics.

- Climate model biases play important roles in the simulation of the relationship between extreme wet/dry conditions and SST variability. More specifically, warm SST biases in the eastern tropical Atlantic are linked to wet biases in precipitation extending over the Congo basin (see Fig. 9b). This represents a too southerly position of the ITCZ, thereby tying the Congo basin to the Atlantic Niño/Niña variability, in the CMIP6 ensemble.

5.2 Policy Implications

This study provides an assessment of the mechanisms driving precipitation extremes over the humid tropical regions, using the 6-month standardized precipitation index, which reflects variations in meteorological and soil moisture conditions. The findings are particularly relevant for the ecosystems, agriculture, and public utilities. We conclude that the accurate simulation of precipitation variability over the

humid tropical regions in state-of-the-art climate models remains a key challenge, most notably over the Congo basin. This calls for the improvements of the seasonal climate prediction models to address the model biases identified in this study, such as the too strong Atlantic cold tongue-Congo basin coupling as well as the region's weak teleconnections to the Indo-Pacific in our multi-model ensemble. The same is true of the asymmetrical impacts of oceanic influences on different humid tropical regions.

Generally speaking, the humid tropics are considered data-scarce regions (e.g., Washington et al. 2006), with particularly low gauge density per grid-cell during the recent decades as shown in Fig. 1e. Thus, enhanced observational systems and internationally-coordinated efforts to reduce the time-lapse before the observations are included in the global archives (Becker et al. 2013) are necessary to address this gap. This study suggests possible low-frequency modulations of the extreme precipitation conditions, with potential implications for long-term climate change. Specifically, the interactions of such modulations with externally-forced climate change, and the weaknesses of the current generation of state-of-the-art climate models highlighted in this study must be carefully considered in climate change adaptation policies for the affected countries.

Author Contributions Conceptualization: HCN, ID; Methodology: HCN, ID; Formal analysis and investigation: HCN; Writing—original draft preparation: HCN, ID; Writing—review and editing: HCN, ID; Resources: HCN, ID.

Data Availability The analyzed CMIP6 outputs are available at: https://esgf-node.llnl.gov/projects/cmip6/. The observational precipitation datasets GPCC: DOI: https://doi.org/10.5676/DWD_GPCC/FD_M_V7_250; CRU: https://crudata.uea.ac.uk/cru/data/hrg/; CHIRPS: https://www.chc.ucsb.edu/data/chirps; CMAP: https://psl.noaa.gov/data/gridded/data.cmap.html; GPCP: https://psl.noaa.gov/data/gridded/data.gpcp.html; observational air temperature: https://psl.noaa.gov/data/gridded/data.UDel_AirT_Precip.html; sea surface temperature: COBE: https://psl.noaa.gov/data/gridded/data.cobe2.html; ERSST: https://psl.noaa.gov/data/gridded/data.noaa.ersst.v5.html; HadISST: https://www.metoffice.gov.uk/hadobs/hadisst/data/download.html; KAPLAN: https://psl.noaa.gov/data/gridded/data.kaplan_sst.html; and twentieth century reanalysis: https://psl.noaa.gov/data/gridded/data.20thC_ReanV3.html are all freely and publicly available from their original sources through the links provided.

Code Availability Not applicable.

Declarations

Conflict of interest The authors declare no potential conflict of interest.

References

Adam O, Schneider T, Brient F (2018) Regional and seasonal variations of the double-ITCZ bias in CMIP5 models. Clim Dyn 51(1–2):101–117. https://doi.org/10.1007/s00382-017-3909-1

Adhikari P, Hong Y, Douglas KR, Kirschbaum DB, Gourley J, Adler R, Brakenridge GR (2010) A digitized global flood inventory (1998–2008): compilation and preliminary results. Nat Hazards 55:405–422. https://doi.org/10.1007/s11069-010-9537-2

Adler RF, Huffman GJ, Chang A, Ferraro R, Xie PP, Janowiak J, Rudolf J, Schneider U, Curtis S, Bolvin D, Gruber A, Susskind J, Arkin P, Nelkin E (2003) The version-2 Global Precipitation Climatology Project (GPCP) monthly precipitation analysis (1979–Present). J Hydrometeorol 4:1147–1167. https://doi.org/10.1175/1525-7541(2003)004%3c1147:TVGPCP%3e2.0.CO;2

Ajayi VO, Ilori OW (2020) Projected drought events over West Africa using RCA4 regional climate model. Earth Syst Environ 4:329–348. https://doi.org/10.1007/s41748-020-00153-x

Almazroui M, Islam MN, Saeed F, Saeed S, Ismail M, Ehsan MA, Diallo I, O'Brien E, Ashfaq M, Martinez-Castro D, Cavazos T, Cerezo-Mota R, Tippett MK, Gutowski WJ Jr, Alfaro EJ, Hidalgo HG, Vichot-llano A, Campbell JD, Kamil S, Rashid IU, Sylla MB, Stephenson T, Taylor M, Barlow M (2021a) Projected changes in temperature and precipitation over the United States, Central America, and the Caribbean in CMIP6 GCMs. Earth Syst Environ 5:1–24. https://doi.org/10.1007/s41748-021-00199-5

Almazroui M, Islam MN, Saeed F et al (2021b) Projected changes in temperature and precipitation over the United States, Central America, and the Caribbean in CMIP6 GCMs. Earth Syst Environ 5:1–24. https://doi.org/10.1007/s41748-021-00199-5

Bader J, Latif M (2003) The impact of decadal-scale Indian Ocean sea surface temperature anomalies on Sahelian rainfall and the North Atlantic oscillation. Geophys Res Lett 30:2169. https://doi.org/10.1029/2003GL018426,22

Baker JCA, Spracklen DV (2022) Divergent representation of precipitation recycling in the Amazon and the Congo in CMIP6 models. Geophys Res Lett 49:e2021GL095136. https://doi.org/10.1029/2021GL095136

Beck H, Zimmermann NE, McVicar TR, Vergopolan N, Berg A, Wood EF (2018) Present and future Köppen–Geiger climate classification maps at 1-km resolution. Sci Data 5:180214. https://doi.org/10.1038/sdata.2018.214

Becker A, Finger P, Meyer-Christoffer A, Rudolf B, Schamm K, Schneider U, Ziese M (2013) A description of the global land-surface precipitation data products of the Global Precipitation Climatology Centre with sample applications including centennial (trend) analysis from 1901-present. Earth Syst Sci Data 5:71–99. https://doi.org/10.5194/essd-5-71-2013

Bi D, Dix M, Marsland S, O'farrell S, Sullivan A, Bodman R, Law R, Harman I, Srbinovsky J, Rashid HA, Dobrohotoff P (2020) Configuration and spin-up of ACCESS-CM2, the new generation Australian Community Climate and Earth System Simulator Coupled Model. J South Hemisph Earth Syst Sci 70(1):225–251. https://doi.org/10.1071/es19040

Bjerknes J (1969) Atmospheric teleconnections from the equatorial Pacific. Mon Weather Rev 97:163–172

Boucher O, Servonnat J, Albright AL, Aumont O, Balkanski Y, Bastrikov V, Bekki S et al (2020) Presentation and evaluation of the IPSL-CM6A-LR climate model. J Adv Model Earth Syst 12(7):e2019MS002010. https://doi.org/10.1029/2019ms002010

Cai W, Wu L, Lengaigne M, Li T, McGregor S, Kug JS, Yu JY, Stuecker MF, Santoso A, Li X, Ham YG, Chikamoto Y, Ng B, McPhaden MJ, Du Y, Dommenget D, Jia F, Kajtar JB, Keenlyside N, Chang P (2019) Pantropical climate interactions. Science 363(6430):1–11. https://doi.org/10.1126/science.aav4236

Cai W, McPhaden MJ, Grimm AM et al (2020) Climate impacts of the El Niño-Southern Oscillation on South America. Nat Rev Earth Environ 1:215–231. https://doi.org/10.1038/s43017-020-0040-3

Chang P, Ji L, Li HA (1997) Decadal climate variation in the tropical Atlantic Ocean from thermodynamic air-sea interactions. Nature 385:516–518

Cherchi A, Fogli PG, Lovato T, Peano D, Lovino D, Gualdi S, Masina S, Scoccimarro E, Materia S, Bellucci A, Navarra A (2019) Global mean climate and main patterns of variability in the CMCC-CM2 coupled model. J Adv Model Earth Syst 11(1):185–209. https://doi.org/10.1029/2018ms001369

Chiang F, Mazdiyasni O, AghaKouchak A (2021) Evidence of anthropogenic impacts on global drought frequency, duration, and intensity. Nat Commun 12:2754. https://doi.org/10.1038/s41467-021-22314-w

Cook KH, Liu Y, Vizy EK (2020) Congo Basin drying associated with poleward shifts of the African thermal lows. Clim Dyn 54:863–883

Cox P et al (2008) Increasing risk of Amazonian drought due to decreasing aerosol pollution. Nature 453(7192):212–215

Da Silva NA, Matthews AJ (2021) Impact of the Madden–Julian oscillation on extreme precipitation over the western Maritime Continent and Southeast Asia. Q J R Meteorol Soc 147(739):3434–3453. https://doi.org/10.1002/qj.4136

Danabasoglu G, Lamarque JF, Bacmeister J, Bailey DA, DuVivier AK, Edwards J, Emmons LK, Fasullo J, Garcia R, Gettelman A, Hannay C, Holland MM, Large WG, Lauritzen PH, Lawrence DM, Lenaerts JTM, Lindsay K, Lipscomb WH, Mills MJ, Neale R, Oleson KW et al (2020) The Community Earth System Model version 2 (CESM2). J Adv Model Earth Syst 12(2):e2019MS001916. https://doi.org/10.1029/2019ms001916

Davey M, Huddleston M, Sperber K, Braconnot P, Bryan F, Chen D, Colman R, Cooper C, Cubasch U, Delecluse P, DeWitt D, Fairhead L, Flato G, Gordon C, Hogan T, Ji M, Kimoto M, Kitoh A, Knutson T, Zebiak S (2002) STOIC: a study of coupled model climatology and variability in tropical ocean regions. Clim Dyn 18(5):403–420. https://doi.org/10.1007/s00382-001-0188-6

De Szoeke SP, Xie SP (2008) The tropical eastern Pacific seasonal cycle: assessment of errors and mechanisms in IPCC AR4 coupled ocean-atmosphere general circulation models. J Clim 21(11):2573–2590. https://doi.org/10.1175/2007jcli1975.1

Dewata I, Umar I (2019) Management of flood hazard areas in Pasaman River basin of West Pasaman Regency, West Sumatra Province. Int J GEOMATE 17:230–237

Dikshit A, Pradhan B, Alamri AM (2020) Short-term spatio-temporal drought forecasting using random forests model at New South Wales, Australia. Appl Sci 10(12):4254

Ding R, Kang I, Farneti R, Kucharski F, Sante FD, Xuan J, Zhou F, Zhang T (2022) The internal and ENSO-forced modes of the Indian Ocean sea surface temperature. J Clim 35:4191–4206. https://doi.org/10.1175/JCLI-D-21-0403.1

Döscher R, Acosta M, Alessandri A, Anthoni P, Arsouze T, Bergman T, Bernardello R, Boussetta S et al (2022) The EC-Earth3 Earth System Model for the Climate Model Intercomparison Project 6. Geosci Model Dev 15:2973–3020. https://doi.org/10.5194/gmd-15-2973-2022,2022

Drumond A, Marengo J, Ambrizzi T, Nieto R, Moreira L, Gimeno L (2014) The role of the Amazon Basin moisture in the atmospheric branch of the hydrological cycle: a Lagrangian analysis. Hydrol Earth Syst Sci 18:2577–2598. https://doi.org/10.5194/hess-18-2577-2014

Dunne JP, Horowitz LW, Adcroft AJ, Ginoux P, Held IM, John JG, Krasting JP, Malyshev S, Naik V, Paulot F et al (2020) The GFDL Earth System Model version 41 (GFDL-ESM 41): overall coupled model description and simulation characteristics. J Adv Model Earth Syst 12(11):e2019MS002015. https://doi.org/10.1029/2019ms002015

Dyer ELE, Jones DBA, Nusbaumer J, Li H, Collins O, Vettoretti G, Noone D (2017) Congo Basin precipitation: assessing seasonality regional interactions, and sources of moisture. J Geophys Res 122:6882–6898

Edwards DC, McKee TB (1997) Characteristics of 20th century drought in the United States at multiple time scales. Climatology Report Number 97-2. Colorado State University, Fort Collins

Erfanian A, Wang G, Fomenko L (2017) Unprecedented drought over tropical South America in 2016: significantly under-predicted by tropical SST. Sci Rep 7:5811. https://doi.org/10.1038/s41598-017-05373-2

Eyring V, Bony S, Meehl GA, Senior CA, Stevens B, Stouffer RJ, Taylor KE (2016) Overview of the Coupled Model Intercomparison Project Phase 6 (CMIP6) experimental design and organization. Geosci Model Dev 9:1937–1958. https://doi.org/10.5194/gmd-9-1937-2016

Eyring V, Gillett NP, Achuta Rao KM, Barimalala R, Barreiro Parrillo M, Bellouin N, Cassou C, Durack PJ, Kosaka Y, McGregor S, Min S, Morgenstern O, Sun Y (2021) Human influence on the climate system. In: Masson-Delmotte V, Zhai P, Pirani A, Connors SL, Péan C, Berger S, Caud N, Chen Y, Goldfarb L, Gomis MI, Huang M, Leitzell K, Lonnoy E, Matthews JBR, Maycock TK, Waterfield T, Yelekçi O, Yu R, Zhou B (eds) Climate change 2021: the physical science basis. Contribution of Working Group I to the sixth assessment report of the Intergovernmental Panel on Climate Change. Cambridge University Press, Cambridge and New York, pp 423–552. https://doi.org/10.1017/9781009157896.005

Farneti R, Stiz A, Ssebandeke JB (2022) Improvements and persistent biases in the southeast tropical Atlantic in CMIP models. Npj Clim Atmos Sci 5:42. https://doi.org/10.1038/s41612-022-00264-4

Fernandes K, Giannini A, Verchot L, Baethgen W, Pinedo-Vasquez M (2015) Decadal covariability of Atlantic SSTs and western Amazon dry-season hydroclimate in observations and CMIP5 simulations. Geophys Res Lett 42:6793–6801. https://doi.org/10.1002/2015GL063911

Foltz GR et al (2019) The tropical Atlantic observing system. Front Mar Sci 6:206. https://doi.org/10.3389/fmars.2019.00206

Funk C, Peterson P, Landsfeld M, Pedreros D, Verdin J, Shukla S, Husak G, Rowland J, Harrison L, Hoell A, Michaelsen J (2015) The climate hazards infrared precipitation with stations—a new environmental record for monitoring extremes. Sci Data 2:150066. https://doi.org/10.1038/sdata.2015.66

Gulizia C, Camilloni I (2015) Comparative analysis of the ability of a set of CMIP3 and CMIP5 global climate models to represent precipitation in South America. Int J Climatol 35:583–595

Gushchina D, Zheleznova I, Osipov A, Olchev A (2020) Effect of various types of ENSO events on moisture conditions in the humid and subhumid tropics. Atmosphere 11(12):1354. https://doi.org/10.3390/atmos11121354

Harris I, Osborn TJ, Jones P, Lister D (2020) Version 4 of the CRU TS monthly high-resolution gridded multivariate climate dataset. Sci Data 7:109. https://doi.org/10.1038/s41597-020-0453-3

Hart NCG, Washington R, Maidment RI (2019) Deep convection over Africa: annual cycle, ENSO, and trends in the hotspots. J Clim 32(24):8791–8811

He B, Yu Y, Bao Q, Lin P, Liu H, Li J, Wang L, Liu Y, Wu G, Chen K, Guo Y, Zhao S, Zhang X, Song M, Xie J (2020) CAS FGOALS-f3-L model dataset descriptions for CMIP6 DECK experiments. Atmos Ocean Sci Lett 13(6):582–588. https://doi.org/10.1080/16742834.2020.1778419

Hewitson BC, Daron J, Crane RG, Zermoglio MF, Jack C (2014) Interrogating empirical-statistical downscaling. Clim Change 122:539–554. https://doi.org/10.1007/s10584-013-1021-z

Hua W, Zhou L, Chen H, Nicholson SE, Raghavendra A, Jiang Y (2016) Possible causes of the Central Equatorial African long-term drought. Environ Res Lett 11:124002

Hua W, Zhou L, Chen H, Nicholson SE, Jiang Y, Raghavendra A (2018) Understanding the central equatorial Africa long-term drought using AMIP-type simulations. Clim Dyn 50:1115–1128

Huang BH, Kinter JL (2002) Interannual variability in the tropical Indian Ocean. J Geophys Res 107:3199. https://doi.org/10.1029/2001JC001278

Huang B, Thorne PW, Banzon VF, Boyer T, Chepurin G, Lawrimore JH, Menne MJ, Smith TM, Vose RS, Zhang H-M (2017) Extended Reconstructed Sea Surface Temperature, version 5 (ERSSTv5): upgrades, validations, and intercomparisons. J Clim 30:8179–8205. https://doi.org/10.1175/JCLI-D-16-0836.1

Huang Y, Wu B, Li T, Zhou T, Liu B (2019) Interdecadal Indian Ocean basin mode driven by interdecadal pacific oscillation: a season-dependent growth mechanism. J Clim 32(7):2057–2073

Ishii M, Shouji A, Sugimoto S, Matsumoto T (2005) Objective analyses of sea-surface temperature and marine meteorological variables for the 20th century using ICOADS and the Kobe collection. Int J Climatol 25:865–879

Kaplan A, Cane M, Kushnir Y, Clement A, Blumenthal M, Rajagopalan B (1998) Analyses of global sea surface temperature 1856–1991. J Geophys Res 103:18567–18589

Kennedy JJ (2014) A review of uncertainty in in situ measurements and data sets of sea surface temperature. Rev Geophys 52:1–32. https://doi.org/10.1002/2013RG000434

Khan AA, Zhao Y, Khan J et al (2021) Spatial and temporal analysis of rainfall and drought condition in Southwest Xinjiang in Northwest China, using various climate indices. Earth Syst Environ 5:201–216. https://doi.org/10.1007/s41748-021-00226-5

Kim IW, Oh J, Woo S et al (2019) Evaluation of precipitation extremes over the Asian domain: observation and modelling studies. Clim Dyn 52:1317–1342. https://doi.org/10.1007/s00382-018-4193-4

Kirono DG, Round V, Heady C, Chiew FHS, Osbrough S (2020) Drought projections for Australia: updated results and analysis of model simulations. Weather Clim Extremes 30:100280

Klein SA, Soden BJ, Lau NC (1999) Remote sea surface temperature variations during ENSO: evidence for a tropical atmospheric bridge. J Clim 12:917–932. https://doi.org/10.1175/1520-0442(1999)012%3c0917:RSSTVD%3e2.0.CO;2

Klutse NAB, Quagraine KA, Nkrumah F et al (2021) The climatic analysis of summer monsoon extreme precipitation events over West Africa in CMIP6 simulations. Earth Syst Environ 5:25–41. https://doi.org/10.1007/s41748-021-00203-y

Kooperman GJ, Chen Y, Hoffman FM, Koven CD, Lindsay K, Pritchard MS, Swann ALS, Randerson JT (2018) Forest response to rising CO2 drives zonally asymmetric rainfall change over tropical land. Nat Clim Change 8:434–440

Latif M, Barnett TP (1995) Interactions of the tropical oceans. J Clim 8:952–964

Lau WKM, Kim K-M, Harrop B, Leung LR (2023) Changing characteristics of tropical extreme precipitation-cloud regimes in warmer climates. Atmosphere 14(6):995. https://doi.org/10.3390/atmos14060995

Lee TH, Lo MH (2021) The role of El Niño in modulating the effects of deforestation in the Maritime Continent. Environ Res Lett. https://doi.org/10.1088/1748-9326/abe88e

Lee J, Kim J, Sun MA, Kim BH, Moon H, Sung HM, Kim J, Byun YH (2020a) Evaluation of the Korea Meteorological Administration Advanced Community Earth-System Model (K-ACE). Asia Pac J Atmos Sci 56(3):381–395. https://doi.org/10.1007/s13143-019-00144-7

Lee W-L, Wang Y-C, Shiu C-J, Tsai I-C, Tu C-Y, Lan Y-Y, Chen J-P, Pan H-L, Hsu H-H (2020b) Taiwan Earth System Model version 1: description and evaluation of mean state. Geosci Model Dev 13(9):3887–3904. https://doi.org/10.5194/gmd-13-3887-2020

Legates DR, Willmott CJ (1990) Mean seasonal and spatial variability in global surface air temperature. Theor Appl Climatol 41:11–21. https://doi.org/10.1007/BF00866198

Li X, Tang Y, Song X, Liu T (2022) Decadal variation of the rainfall predictability over the maritime continent in the wet season. J Clim 35:4859–4867. https://doi.org/10.1175/JCLI-D-21-0862.1

Ling J, Zhang C (2013) Diabatic heating profiles in recent global reanalyses. J Clim 26(10):3307–3325

Lübbecke JF, Rodríguez-Fonseca B, Richter I, Martin-Rey M, Losada T, Polo I, Keenlyside NS (2018) Equatorial Atlantic variability—modes, mechanisms, and global teleconnections. Wires Clim Change 9(4):e527. https://doi.org/10.1002/wcc.527

Lüdecke H, Müller-Plath G, Wallace MG, Lüning S (2021) Decadal and multidecadal natural variability of African rainfall. J Hydrol Reg Stud 34:100795. https://doi.org/10.1016/j.ejrh.2021.100795

Marengo JA (1992) Interannual variability of surface climate in the Amazon basin. Int J Climatol 12:853–863. https://doi.org/10.1002/joc.3370120808

Marengo J (2004) Interdecadal variability and trends of rainfall across the Amazon basin. Theor Appl Climatol 78:79–96. https://doi.org/10.1007/s00704-004-0045-8

Marengo JA, Espinoza JC (2016) Extreme seasonal droughts and floods in Amazonia: causes, trends and impacts. Int J Climatol 36:1033–1050. https://doi.org/10.1002/joc.4420

Marengo J et al (2011) The drought of 2010 in the context of historical droughts in the Amazon region. Geophys Res Lett 38(12):1–5

Mauritsen T, Bader J, Becker T, Behrens J, Bittner M, Brokopf R, Brovkin V, Claussen M, Crueger T, Esch M, Fast I, Fiedler S, Flaschner D, Gayler V, Giorgetta M, Goll DS, Haak H et al (2019) Developments in the MPI-M Earth System Model version 1.2 (MPI-ESM1.2) and its response to increasing CO$_2$. J Adv Model Earth Syst 11(4):998–1038. https://doi.org/10.1029/2018ms001400

McKee TB, Doesken NJ, Kleist J (1993) The relationship of drought frequency and duration to time scales. In: Proceedings of the 8th conference on applied climatology, 17–22 January 1993, Anaheim, CA. American Meteorological Society, Boston

McPhaden et al (2006) ENSO as an integrating concept in earth science. Science 314:1740–1745

Mechoso CR, Robertson AW, Barth N, Davey MK, Delecluse P, Gent PR, Ineson S, Kirtman B, Latif M, Treut HL, Nagai T, Neelin JD, Philander SGH, Polcher J, Schopf PS, Stockdale T, Suarez MJ, Terray L, Thual O, Tribbia JJ (1995) The seasonal cycle over the tropical Pacific in coupled ocean-atmosphere general-circulation models. Mon Weather Rev 123(9):2825–2838. https://doi.org/10.1175/1520-0493(1995)123%3c2825:tscott%3e2.0.co;2

Milinski S, Bader J, Haak H, Siongco AC, Jungclaus JH (2016) High atmospheric horizontal resolution eliminates the wind-driven coastal warm bias in the southeastern tropical Atlantic. Geophys Res Lett 43:10455–10462. https://doi.org/10.1002/2016GL070530

Mizuta R, Yoshimura H, Murakami H, Matsueda M, Endo H, Ose T, Kamiguchi K, Hosaka M, Sugi M, Yukimoto S, Kusunoki S (2012) Climate simulations using MRI-AGCM3.2 with 20-km grid. J Meteorol Soc Jpn Ser II 90A:233–258. https://doi.org/10.2151/jmsj.2012-a12

Mohammed UD, Legesse SA, Berlie AB et al (2022) Climate change repercussions on meteorological drought frequency and intensity in South Wollo, Ethiopia. Earth Syst Environ 6:645–655. https://doi.org/10.1007/s41748-022-00293-2

Moihamette F, Pokam WM, Diallo I, Washington R (2022) Extreme Indian Ocean dipole and rainfall variability over Central Africa. Int J Climatol 42(10):5255–5272

Müller WA, Jungclauss JH, Mauritsen T, Baehr J, Bittner M, Budich R, Bunzel F, Esch M, Ghosh R, Haak H, Ilyina T, Kleine T, Kornblueh L, Li H, Modali K, Notz D, Pohlmann H, Roeckner E, Stemmler I, Tian F, Marotzke J (2018) A higher-resolution version of the Max Planck Institute Earth System Model (MPI-ESM1.2-HR). J Adv Model Earth Syst 10(7):1383–1413. https://doi.org/10.1029/2017ms001217

Nicholson SE (2009) A revised picture of the structure of the "monsoon" and land ITCZ over West Africa. Clim Dyn 32:1155–1171. https://doi.org/10.1007/s00382-008-0514-3

Nicholson S, Klotter DA, Zhou L, Hua W (2022) Recent rainfall conditions in the Congo basin. Environ Res Lett 17:054052

Nnamchi HC, Latif M, Keenlyside NS, Kjellson J, Richter I (2021) Diabatic heating governs the seasonality of the Atlantic Niño. Nat Commun 12:376. https://doi.org/10.1038/s41467-020-20452-1

Nnamchi HC, Farneti R, Keenlyside NS et al (2023) Pan-Atlantic decadal climate oscillation linked to ocean circulation. Commun Earth Environ 4:121. https://doi.org/10.1038/s43247-023-00781-x

Parker DE, Jones PD, Folland CK, Bevan A (1994) Interdecadal changes of surface temperature since the late nineteenth century. J Geophys Res 99:14373–14399

Philander et al (1984) Unstable air–sea interactions in the tropics. J Atmos 41:604–613

Phuong DND, Hai LM, Dung HM et al (2022) Temporal trend possibilities of annual rainfall and standardized precipitation index in the Central Highlands, Vietnam. Earth Syst Environ 6:69–85. https://doi.org/10.1007/s41748-021-00211-y

Rayner NA, Parker DE, Horton EB, Folland CK, Alexander LV, Rowell DP, Kent EC, Kaplan A (2003) Global analyses of sea surface temperature, sea ice, and night marine air temperature since the late nineteenth century. J Geophys Res 108(D14):4407. https://doi.org/10.1029/2002JD002670

Richter I, Tokinaga H (2020) An overview of the performance of CMIP6 models in the tropical Atlantic: mean state, variability, and remote impacts. Clim Dyn 55:2579–2601. https://doi.org/10.1007/s00382-020-05409-w

Richter I, Xie SP (2008) On the origin of equatorial Atlantic biases in coupled general circulation models. Clim Dyn 31:587–598. https://doi.org/10.1007/s00382-008-0364-z

Richter I, Xie SP, Behera SK et al (2014) Equatorial Atlantic variability and its relation to mean state biases in CMIP5. Clim Dyn 42:171–188. https://doi.org/10.1007/s00382-012-1624-5

Robinson A, Lehmann J, Barriopedro D et al (2021) Increasing heat and rainfall extremes now far outside the historical climate. Npj Clim Atmos Sci 4:45. https://doi.org/10.1038/s41612-021-00202-w

Roca R, Fiolleau T (2020) Extreme precipitation in the tropics is closely associated with long-lived convective systems. Commun Earth Environ 1:18. https://doi.org/10.1038/s43247-020-00015-4

Rodysill JR, Russell JM, Vuille M, Dee S, Lunghino B, Bijaksana S (2019) La Niña-driven flooding in the Indo-Pacific warm pool during the past millenium. Quat Sci Rev 225:106020. https://doi.org/10.1016/j.quascirev.2019.106020

Ropelewski CF, Halpert MS (1987) Global and regional scale precipitation patterns associated with the El Niño/Southern Oscillation. Mon Weather Rev 115:1606–1626

Rowland L, Da Costa ACL, Galbraith DR, Oliveira RS, Binks OJ, Oliveira AAR, Pullen AM, Doughty CE, Metcalfe DB, Vasconcelos SS (2015) Death from drought in tropical forests is triggered by hydraulics not carbon starvation. Nature 528:119–122

Saji NH, Yamagata T (2003) Structure of SST and surface wind variability during Indian Ocean dipole mode events: COADS observations. J Clim 16:2735–2751

Schneider U, Becker A, Finger P et al (2014) GPCC's new land surface precipitation climatology based on quality-controlled in situ data and its role in quantifying the global water cycle. Theor Appl Climatol 115:15–40. https://doi.org/10.1007/s00704-013-0860-x

Schneider U, Finger P, Meyer-Christoffer A, Rustemeier E, Ziese M, Becker (2017) Evaluating the hydrological cycle over land using the newly-corrected precipitation climatology from the Global Precipitation Climatology Centre (GPCC). Atmosphere. https://doi.org/10.3390/atmos8030052

Schott FA, Xie SP, McCreary JP (2009) Indian Ocean circulation and climate variability. Rev Geophys 47:RG1002. https://doi.org/10.1029/2007RG000245

Seland Ø, Bentsen M, Olivie D et al (2020) Overview of the Norwegian Earth System Model (NorESM2) and key climate response of CMIP6 DECK, historical, and scenario simulations. Geosci Model Dev 13(12):6165–6200. https://doi.org/10.5194/gmd-13-6165-2020

Semmler T, Danilov S, Gierz P, Goessling HF, Hegewald J, Hinrichs C, Koldunov N, Khosravi N, Mu L, Rackow T, Sein DV, Sidorenko D, Wang Q, Jung T (2020) Simulations for CMIP6 with the AWI climate model AWI-CM-1-1. J Adv Model Earth Syst 12(9):e2019MS002009. https://doi.org/10.1029/2019ms002009

Seneviratne S et al (2012) Changes in climate extremes and their impacts on the natural physical environment. Managing the risks of extreme events and disasters to advance climate change adaptation. Cambridge University Press, Cambridge and New York

Servain J, Wainer I, McCreary JP Jr, Dessier A (1999) Relationship between the equatorial and meridional modes of climatic variability in the Tropical Atlantic. Geophys Res Lett 26(4):485–488. https://doi.org/10.1029/1999gl900014

Sharma S, Hamal K, Khadka N et al (2021) Projected drought conditions over southern slope of the Central Himalaya using CMIP6 models. Earth Syst Environ 5:849–859. https://doi.org/10.1007/s41748-021-00254-1

Shi J, Cui L, Tian Z (2020) Spatial and temporal distribution and trend in flood and drought disasters in East China. Environ Res Lett 185:109406

Sidorenko D, Rackow T, Jung T, Semmler T, Barbi D, Danilov S, Dethloff K et al (2015) Towards multi-resolution global climate modelling with ECHAM6–FESOM. Part I: model formulation and mean climate. Clim Dyn 44(3):757–780. https://doi.org/10.1007/s00382-014-2290-6

Slivinski LC et al (2019) Towards a more reliable historical reanalysis: improvements for version 3 of the Twentieth Century Reanalysis system. Quart J Roy Meteorol Soc 145:2876–2908. https://doi.org/10.1002/qj.3598

Stechmann SN, Ogrosky HR (2014) The Walker circulation, diabatic heating, and outgoing longwave radiation. Geophys Res Lett 41:9097–9105. https://doi.org/10.1002/2014GL062257

Strnad FM, Schlör J, Geen R et al (2023) Propagation pathways of Indo-Pacific rainfall extremes are modulated by Pacific sea surface temperatures. Nat Commun 14:5708. https://doi.org/10.1038/s41467-023-41400-9

Swart NC et al (2019) The Canadian Earth System Model version 5 (CanESM503). Geosci Model Dev 12(11):4823–4873. https://doi.org/10.5194/gmd-12-4823-2019

Tamoffo AT et al (2019) Process-oriented assessment of RCA4 regional climate model projections over the Congo Basin under 1.5 °C and 2 °C global warming levels: influence of regional moisture fluxes. Clim Dyn 53:1911–1935

Tatebe H et al (2019) Description and basic evaluation of simulated mean state, internal variability, and climate sensitivity in MIROC6. Geosci Model Dev 12(7):2727–2765. https://doi.org/10.5194/gmd-12-2727-2019

Tian B, Dong X (2020) The double-ITCZ Bias in CMIP3, CMIP5 and CMIP6 models based on annual mean precipitation. Geophys Res Lett 47:e2020GL087232. https://doi.org/10.1029/2020GL087232

Towner J, Cloke HL, Lavado W et al (2020) Attribution of Amazon floods to modes of climate variability: a review. Meteorol Appl 27:e1949. https://doi.org/10.1002/met.1949

Villamayor J, Ambrizzi T, Mohino E (2018) Influence of decadal sea surface temperature variability on northern Brazil rainfall in CMIP5 simulations. Clim Dyn 51:563–579

Volodin EM, Mortikov EV, Kostrykin SV, Galin V, Lykossov VN, Gritsun AS, Diansky NA, Gusev AV, Lakovlev NG (2017) Simulation of the present-day climate with the climate model INMCM5. Clim Dyn 49(11):3715–3734. https://doi.org/10.1007/s00382-017-3539-7

Wang C (2002) Atmospheric circulation cells associated with the El Niño-Southern oscillation. J Clim 15:399–419. https://doi.org/10.1175/1520-0442(2002)015%3c0399:ACCAWT%3e2.0.CO;2

Wang G, Sun S, Mei R (2011) Vegetation dynamics contributes to the multi-decadal variability of precipitation in the Amazon region. Geophys Res Lett. https://doi.org/10.1029/2011GL049017

Wang XY, Zhu J, Xin M et al (2021) Weakened seasonality of the African rainforest precipitation in boreal winter and spring driven by tropical SST variabilities. Geosci Lett 8:22. https://doi.org/10.1186/s40562-021-00192-w

Washington R et al (2006) African climate change: taking the shorter route. Bull Am Meteorol Soc 87:1355–1366. https://doi.org/10.1175/BAMS-87-10-1355

Washington R, James R, Pearce H, Pokam WM, Moufouma-Okia W (2013) Congo basin rainfall climatology: can we believe the climate models? Philos Trans Roy Soc Lond Ser B. https://doi.org/10.1098/rstb.2012.0296

Webster PJ (1983) Large-scale structure of the tropical atmosphere. In: Hoskins B, Pearce R (eds) Large scale dynamical processes in the atmosphere. Academic Press, New York, pp 235–275

Weng H, Behera SK, Yamagata T (2009) Anomalous winter climate conditions in the Pacific rim during recent El Niño Modoki and El Niño events. Clim Dyn 32:663–674. https://doi.org/10.1007/s00382-008-0394-6

Willmott CJ, Matsuura K (1995) Smart interpolation of annually averaged air temperature in the United States. J Appl Meteorol Climatol 34(12):2577–2586

World Meteorological Organization (2012) Standardized precipitation index user guide (WMO-No.1090), Geneva

Wu T et al (2019) The Beijing Climate Center Climate System Model (BCC-CSM): the main progress from CMIP5 to CMIP6. Geosci Model Dev 12(4):1573–1600. https://doi.org/10.5194/gmd-12-1573-2019

Xiao HM, Lo MH, Yu JY (2022) The increased frequency of combined El Niño and positive IOD events since 1965s and its impacts on

maritime continent hydroclimates. Sci Rep 12:7532. https://doi.org/10.1038/s41598-022-11663-1

Xie P, Arkin PA (1997) Global precipitation: a 17-year monthly analysis based on gauge observations, satellite estimates, and numerical model outputs. Bull Am Meteorol Soc. https://doi.org/10.1175/1520-0477(1997)078%3c2539:GPAYMA%3e2.0.CO;2

Xie SP, Tanimoto YA (1998) A pan-Atlantic decadal climate oscillation. Geophys Res Lett 25(12):2185–2188. https://doi.org/10.1029/98GL01525

Xie Z, Duan A, Tian Q (2017) Weighted composite analysis and its application: an example using ENSO and geopotential height. Atmos Sci Lett 18:435–440. https://doi.org/10.1002/asl.786

Xu Z, Chang P, Richter I et al (2014) Diagnosing southeast tropical Atlantic SST and ocean circulation biases in the CMIP5 ensemble. Clim Dyn 43:3123–3145. https://doi.org/10.1007/s00382-014-2247-9

Yanai M, Esbensen S, Chu JH (1973) Determination of bulk properties of tropical cloud clusters from large-scale heat and moisture budgets. J Atmos Sci 30(4):611–627

Yoon J-H (2016) Multi-model analysis of the Atlantic influence on Southern Amazon rainfall. Atmos Sci Lett 17:122–127. https://doi.org/10.1002/asl.600

Yukimoto S, Hideaki K, Tsuyoshi K, Naga O, Kohei Y, Shogo U, Hiroyuki T, Makoto D, Taichu T, Masahiro H, Shokichi Y, Hiromasa Y, Eiki S, Ryo M, Atsushi O, Yukimasa A, Masayoshi I (2019) The Meteorological Research Institute Earth System Model version 2.0, MRI-ESM2.0: description and basic evaluation of the physical component. J Meteorol Soc Jpn Ser II 97(5):931–965. https://doi.org/10.2151/jmsj.2019-051

Zebiak SE (1993) Air–sea interaction in the equatorial Atlantic region. J Clim 6:1567–1586

Zheleznova IV, Gushchina DY (2017) Hadley and Walker circulation anomalies associated with the two types of El Niño. Russ Meteorol Hydrol 42:625–634. https://doi.org/10.3103/S1068373917100016

Ziehn T, Chamberlain MA, Law RM, Lenton A, Bodman RW, Dix M, Stevens L, Wang YP, Srbinovsky J (2020) The Australian Earth System Model: ACCESS-ESM1.5. J South Hemisph Earth Syst Sci 70:193–214. https://doi.org/10.1071/es19035